Observational Study

Medicine

OPEN

The chemical composition analysis of Yixin Tongmai Granules using UHPLC-MS/MS and exploration of its potential mechanism in treatment of coronary artery disease based on network pharmacology and molecular docking

Hongbin Li, PhD[a,*], Yuye Zhu, MD[a]

Abstract

Yixin Tongmai Granules (YTG) is a popular Chinese herbal granules for the treatment of coronary artery disease (CAD), but its molecular pharmacological mechanism is still unclear. This article explores the mechanism of CAD treatment from the perspective of network pharmacology. We analyzed the chemical composition of YTG using UHPLC-MS/MS and identified 131 ingredients. The relative drug content of 33 ingredients exceeded 0.5%. These ingredients were further screened using the SwissADME platform with ADME criteria. Using the HIT database and SwissTargetPrediction platform, high probability targets for these ingredients were generated. Using Venn Diagram, 96 effective targets associated with CAD were identified, involving 14 core ingredients. This study imported these effective targets into the STRING platform and obtained the core targets through network topology analysis: TP53, STAT3, transcription factor Jun, MAPK3, MAPK1, AKT1, SRC, MYC, BCL2, transcription factor p65, TNF, and ESR2. Then enrichment analysis with Metascape platform indicated that, in the system network of YTG in anti-CAD, the principal pathways are "Lipid and Atherosclerosis", "Pathways in cancer", and "AGE-RAGE signaling pathway in diabetic complications." Next, the affinities between the core ingredients and their associated core targets were examined individually through molecular docking. Finally, based on deep mining of PubMed literature, this study investigated the relationship between each core target and CAD, the relationship between each core target and its associated core ingredients, and inferred the main pharmacological ingredients of YTG, namely Tanshinone IIA, Cryptotanshinone, Caffeic acid, Denshensu, Ononin, and Formononetin.

Abbreviations: 2D = 2 dimensional, 3D = 3 dimensional, ACE = angiotensin-converting enzyme, ADME = absorption distribution metabolism excretion, AGC = automatic gain control, AKT1 = serine/threonine kinase 1, AP-1 = adaptor protein complex-1, APOB = apolipoprotein B, APOE = apolipoprotein E, ATP = adenosine triphosphate, BC = before christ, BCL2 = B-cell lymphoma-2, BID = BH3-interacting domain death agonist, CAD = coronary artery disease, CASP3 = caspase-3, CASP8 = caspase-8, CYP1A1 = cytochrome P450 1A, CYP2C9 = cytochrome P450 2C9, DNA = deoxyribonucleic acid, E2 = 17β-estradiol, ERK = extracellular regulated protein kinases, ESR1 = estrogen receptor 1, ESR2 = estrogen receptor 2, FGF2 = fibroblast growth factor 2, FGFR2 = fibroblast growth factor receptor 2, GBD = Global Burden of Disease, GEO = gene expression omnibus, GO = gene ontology, HBV = hepatitis B virus, I/R = ischemia-reperfusion, ICAM1 = intercellular adhesion molecule 1, IL-1β = interleukin-1β, JUN = transcription factor Jun, KEGG = Kyoto Encyclopedia of Genes and Genomes, LDL = low-density lipoprotein, LPS = lipopolysaccharide, MAPK = mitogen-activated protein kinase, MAPK1 = MAP kinase-activated protein kinase 1, MAPK14 = MAP kinase-activated protein kinase 14, MAPK3 = MAP kinase-activated protein kinase 3, MAPK8 = MAP kinase-activated protein kinase 8, MMP1 = matrix metalloproteinase-1, MMP9 = matrix metalloproteinase-9, mRNA = messenger ribonucleic acid, MS = mass spectrometry, MS-dd = full MS/data-dependent, MYC = myelocytomatosis, NFE2L2 = nuclear factor erythroid 2-related factor 2, NFKBIA = NF-kappa-B inhibitor alpha, NLRP3 = NACHT, LRR and PYD domains-containing protein 3, NOS3 = nitric oxide synthase 3, OLR1 = oxidized low-density lipoprotein receptor 1, PDB = Protein Data Bank, PPARG = peroxisome proliferator-activated receptor gamma, PPI = protein–protein interaction, SRC = c-Src, SELP = Selenoprotein P, SMILES = Simplified molecular input line entry system, STAT3 = signal transducer and activator of transcription 3, RELA = transcription factor p65, T2DM = type 2 diabetes mellitus, TCM = traditional Chinese medicine, TIC = total ion chromatography, TLR4 = Toll-like receptor 4, TNF = tumor necrosis factor, TP53 = tumor protein 53, UHPLC-MS/MS = ultra-high performance liquid chromatography tandem mass spectrometry, VCAM1 = vascular cell adhesion molecule 1, VSMC = vascular smooth muscle cells, WHO = world health organization, YTG = Yixin Tongmai Granules.

Keywords: coronary artery disease, molecular docking, network pharmacology, UHPLC-MS/MS, Yixin Tongmai Granules

This study was supported by the doctoral research start-up fund project of Xianyang Polytechnic Institute of People's Republic of China, "Application of information and automation technology in biological medicine" (2021BK07). This study was also supported by the scientific research and innovation team program of Xianyang Polytechnic Institute of People's Republic of China, "Healthcare and Elderly Care Innovation Research Team" (CX202105).

The authors have no conflicts of interest to disclose.

All data generated or analyzed during this study are included in this published article [and its supplementary information files].

1. Introduction

With the aging of society, increasing social pressure, changes in lifestyle and dietary habits, and intensification of air pollution, the incidence of cardiovascular diseases is gradually increasing. Coronary artery disease (CAD) is a chronic heart disease caused by myocardial ischemia and hypoxia due to stenosis or obstruction of the arterial lumen caused by coronary atherosclerosis; angina pectoris is the most common symptom. According to data from the Global Burden of Disease (GBD) database, the global prevalence of CAD in 2016 was 154 million.[1] The high-risk population is a crowd aged over 40 years. The incidence rate of this disease increases with age, with more men than women, most of whom are mental workers. Based on the naming and diagnostic criteria published by the WHO in 1979,[2] the disease can be divided into 4 categories according to its severity: silent coronary heart disease, angina pectoris, myocardial infarction, and ischemic cardiomyopathy. Its main risk factors are dyslipidemia, hypertension, obesity, hyperfibrinoidemia, diabetes, smoking, drinking, high-calorie diet, and lack of exercise.[3] Clinically, CAD treatment is mainly determined by the degree of vascular stenosis. If the stenosis is <75%, it can be controlled with long-term oral medication. However, when the stenosis is more than 75%, it usually requires surgical treatment, such as the use of stent implantation to recover the blood flow perfusion of the stenosed or occluded artery, or vascular bypass surgery to recover the blood supply to the ischemic myocardium. Patients with CAD, whether they have received interventional surgery and revascularization, need to take drugs following the doctor's advice continuously for a long time to improve their quality of life and reduce the risk of death. According to the difference and severity of patients' diseases, drugs often used in clinical medicine for CAD can be divided into the following categories: antiplatelet drugs,[4] such as aspirin and clopidogrel; ester-lowering drugs,[5] such as statins, ezetimibe, fibrates, and nicotinic acids; ACE inhibitors,[6] such as captopril and enalapril; calcium channel blockers,[7] such as nifedipine, and nimodipine; β receptor blockers,[8] such as metoprolol tartrate and atenolol; vasodilator therapy drugs,[9] such as nitroglycerin and isosorbide mononitrate; anticoagulant drugs,[10] such as heparin; and thrombolytic drugs,[11] such as urokinase and streptokinase.

Traditional Chinese medicine (TCM) originated in China's primitive society and was formed during the Zhou dynasty period (1046 BC–256 BC). It has been the accumulated experience of the ancient Chinese people in fighting diseases for thousands of years. It is also a medical theory system that gradually develops through long-term medical practice. Traditional preparations of TCM include decoction, pills, powder, cream, wine, and tea, whereas modern preparations include oral liquids, tablets, soft capsules, granules, drop pills, aerosols, and injections. Granules are made from TCM slices through extraction, concentration, and drying. TCM granules retain the main active ingredients of the TCM formula, and avoid the trouble of boiling TCM. TCM has a long history of cognition with CAD, which belongs to the disease category of "Chest Obstruction" in TCM, which was first seen in the volume of "Lingshu·Benzang" from the monumental work of "Huangdi Neijing." TCM theory states that the occurrence of CAD is related to many factors, such as weakness of the viscera, improper diet, germ infection, emotional disorders, and overwork. In terms of treatment, it adds some natural drugs that can conventionally promote blood circulation and dissipate blood stasis, and it also adds some natural products that can improve heart function and increase the cardiac ejection fraction in patients with severe CAD.

YTG is a commonly used granule-TCM for CAD and angina pectoris developed by Henan Furrentang Pharmaceutical Co., Ltd in China. YTG first appeared in the V2005 edition of the Pharmacopoeia of China and was included in the subsequent pharmacopoeias. It contains 8 herbs: Radix Astragali, Radix Ginseng, Radix Glehniae, Radix Scrophulariae, Radix Salviae miltiorrhizae, Rhizome Chuanxiong, Radix Curcumae, and Radix Glycyrrhizae Preparata. Radix Astragali (huangqi) is the dried root of the leguminous plant *Astragalus membranaceus (Fisch.) Bge*. or *Astragalus membranaceus (Fisch.) Bge. var. mongholicus (Bge.) Hsiao*. Radix Ginseng (renshen) is the dried root of *Panax ginseng C. A. Mey.*, a plant belonging to the Araliaceae family. Radix Glehniae (beishashen) is the dried root of *Glehnia littoralis Fr. Schmidt ex Miq*. in the Umbelliferae family. Radix Scrophulariae (xuanshen) is the dried root of *Scrophularia ningpoensis Hemsl*. in the Scrophulariaceae family. Radix Salviae miltiorrhizae (danshen), the dried root and rhizome of *Salvia miltiorrhiza Bge*., is a Labiatae plant. Rhizome Chuanxiong (chuanxiong), the dried rhizome of *Ligusticum chuanxiong Hort*., belongs to the Umbelliferae family. Radix Curcumae (yujin) is the steamed and dried tuberous root of *Curcuma wenyujin Y. H. Chen et C.Ling,* belonging to Zingiberaceae family. Radix Glycyrrhizae Preparata (zhigancao) is the dried root and rhizome of the leguminous plant *Glycyrrhiza uralensis Fisch*. or *Glycyrrhiza glabra L*., which were processed by stir-baking with honey. YTG can alleviate angina pectoris caused by blood stasis, and can also alleviate symptoms such as fatigue, shortness of breath, and palpitation.[12] Su and He found that YTG can reduce post-surgery restenosis and improper perfusion after PCI to promote patients recovery.[13]

This study adopted TCM analytical chemistry experiments and network pharmacology methods to explore the molecular mechanisms of YTG in anti-CAD. Network pharmacology is a developing discipline based on the theories of system biology and multidirectional pharmacology. It uses computer software and network databases to study and integrate the network relationships between drug ingredients, action targets, signaling pathways, and diseases. Furthermore, it is often used to conduct pharmacological research on drugs, especially natural drugs with complex chemical compositions, thereby guiding the discovery of new medicines. Professor Li Shao, a famous Chinese scholar at Tsinghua University, first proposed a hypothesis of the relationship between TCM and biomolecular networks in 1999. Hopkins, a pharmacologist at Dundee University in the United Kingdom, formally proposed the term 'network pharmacology' in a paper published in the journal Nature Biotechnology in October 2007.[14] The research process

This paper does not involve human, animal, or cell experiments. The data comes from drug composition analysis experiments and some databases, and does not address issues related to patient ethics, etc. Therefore, this study does not require approval by the ethics committee.

Supplemental Digital Content is available for this article.

[a] *Medical School, Xianyang Polytechnic Institute, Xixian New Area, Xi'an, Shaanxi, P.R. China.*

** Correspondence: Hongbin Li, Medical School, Xianyang Polytechnic Institute, #1, Tongyi Road, Xixian New Area, Shaanxi 712000, P.R. China (e-mail: leehbin@126.com).*

How to cite this article: Li H, Zhu Y. The chemical composition analysis of Yixin Tongmai Granules using UHPLC-MS/MS and exploration of its potential mechanism in treatment of coronary artery disease based on network pharmacology and molecular docking. Medicine 2025;104:8(e41620).

Received: 1 June 2024 / Received in final form: 31 January 2025 / Accepted: 3 February 2025

http://dx.doi.org/10.1097/MD.0000000000041620

Table 1

The specific gradient elution conditions.

Time	Flow rate(mL/min）	%A	%B
0	0.3	100	0
10	0.3	70	30
25	0.3	60	40
30	0.3	50	50
40	0.3	30	70
45	0.3	0	100
60	0.3	0	100
60.5	0.3	100	0
70	0.3	100	0

of network pharmacology mainly includes the following steps: obtaining the ingredients of TCM, predicting the corresponding targets of each ingredient, obtaining the targets of disease, taking the intersection of 2 types of targets, constructing the interaction network between the intersection target proteins, carrying out gene ontology and Kyoto Encyclopedia of Genes and Genomes (KEGG) enrichment analysis, and initially revealing TCM action mechanisms for treating certain disease. Molecular docking[15] is not only a common method for new drug design, but also a validation method for network pharmacology research. It is based on structural and molecular biology, which simulates the interaction between ligand and receptor molecules using software. There are 3 commonly used docking modes: rigid docking (both molecules are considered rigid bodies), semi-flexible docking (the ligand molecule is considered a flexible body, and the receptor molecule is considered a rigid body), and flexible docking (both molecules are considered flexible bodies). The docking result, that is, the score of affinity of 2 molecules in a specific relative spatial position, is in the light of comprehensive assessment of geometric complementarity, energetic complementarity and chemical complementarity. Molecular docking software often uses artificial neural networks,[16] support vector machines,[16] deep learning,[16] genetic algorithms,[17] simulated annealing,[18] decision tree[19] or other algorithms to search for the optimal docking conformation of ligand and receptor, and predict their binding mode and affinity.

2. Materials and methods

The key elements of study design in the paper are: analytical chemistry experiments, network pharmacology, molecular docking, and literature review.

2.1. Drug sample processing before chemical analysis

The processing steps for the drug sample before analysis included: take an appropriate amount of sample and place it in a 15mL centrifuge tube; add 10mL of 50% methanol aqueous solution and sonicate for 30 minutes; take 1mL of the supernatant and place it in the centrifuge tube; centrifuge at 14,000 rpm for 5 minutes; filter the supernatant with a microporous membrane (0.22μm); place it in a chromatographic sample bottle and analyze it using UHPLC-MS/MS. The blank sample was treated under the same conditions.

2.2. Experimental instruments of analytical chemistry

The instruments used for the component analysis of TCM included: Orbitrap (Q Exactive Plus; Thermo Fisher, Waltham), ultra-high performance liquid chromatography and automatic sampler (U3000;Thermo Fisher), vortexers (Vortex-2 Genie; Scientific Industries, Bohemia), low temperature centrifuge (5810R; Eppendorf, Free and Hanseatic City of Hamburg, Germany), ultrasonic cleaner (WD-9415C; Beijing Liuyi Instrument Factory, Fangshan, Bejing, China) and chromatographic column (ACQUITY UPLC HSS T3, 2.1 × 100mm, 1.8μm; Waters, Milford).

2.3. Experimental condition

The liquid phase conditions included: the column temperature was set to 35°C; the injection volume was set to 10μL; the velocity of flow was set to 0.3 mL/min; gradient elution was applied in experiment, as shown in Table 1; the mobile phase A used the deionized water containing 0.1% formic acid, while mobile phase B used acetonitrile containing 0.1% formic acid. The mass spectrometry conditions included: the detection mode was set to full MS/data-dependent (MS-dd) MS^2; scanning mode was set to separate scanning (positive ion and negative ion), and scanning range (m/z) was set to 100 to 1500; MS^1 resolution was set to 70,000, and MS^2 resolution was set to 17,500; the ion source voltage was set to 3.2kV; capillary temperature was set to 320 °C; auxiliary gas heater temperature was set to 350 °C; sheath gas flow rate was set to 40L/min; auxiliary gas flow rate was set to 15L/min; AGC Target was set to 1,000,000; TopN was set to 5; the collision energy that triggered MS^2 scanning adopted a stepped fragmentation voltage.

2.4. Obtain the ingredients of YTG, and carry on ADME screening of the ingredients

The feature peaks of the raw mass spectrometry data were extracted using Compound Discoverer software 3.3, and the mass deviation of feature peak element matching, molecular formula prediction, and isotope distribution matching were set to 5ppm. Feature peak identification was performed using the mzCloud online database (http://www.mzcloud.org/) and the locally built TCM natural product database mzVault. The screening criteria for positive ingredients were: mass deviation <5ppm, the matching score with the 2 databases larger than 70, and manual deletion of duplicate results. Due to the insignificant pharmacodynamics of ingredients with low content, this study selected positive ingredients with relative content >0.5%. The names of the positive ingredients with higher content were inputted into the PubChem network platform (https://pubchem.ncbi.nlm.nih.gov/) to obtain their Canonical SMILES formula. Next, Each Canonical SMILES formula for positive ingredients was introduced into the SwissADME[20] network platform (http://www.swissadme.ch/). On the platform, the above ingredients were further screened according to the ADME parameter values. The basis for screening was as follows: at least 2 of the 5 parameters of Lipinski violation, Ghose violation, Veber violation, Egan violation, and Muege violation had a value of zero, and the parameter value of the bioavailability score was greater than or equal to 0.5.

2.5. Predict the effective targets of YTG in anti-CAD

This study used HIT[21] (http://hit2.badd-cao.net/) and SwissTargetPrediction[22] (http://www.swisstargetprediction.ch/) network platforms to carry out strict prediction and collection of the targets of the ingredients that passed the screening above in YTG. The targets of an ingredient provided by HIT are based on the mining of literature; that is, each target of the ingredient is supported by at least 1 of the latest literature evidences, and is classified as direct or indirect inhibitors/activators, binders, and enzymes. However, the target probability prediction of SwissTargetPrediction is based on the measurement of 2D and 3D chemical structure similarities with known ligand molecules. In this study, the ingredient name or its SMILES formula was inputted into the HIT to obtain its targets with literature

evidence. In addition, as a supplement to HIT, predictive targets whose probability was not lower than the threshold (50%) were collected using SwissTargetPrediction. Then, the targets from the 2 platforms meeting the above requirements were merged using EXCEL as the target dataset of YTG. Next, with the key words of "coronary artery disease" and "coronary heart disease" successively, the disease targets of CAD were downloaded from the disease database GeneCards[23] (https://www.genecards.org/) respectively, and were merged by EXCEL. Finally, the drug prediction targets and CAD disease-related targets from the 2 files above were imported into Venny 2.1 (http://www.liuxiaoyuyuan.cn/), a network mapping tool for building a Venn diagram; thus, the intersection target dataset (the effective targets set of YTG anti-CAD) was obtained.

2.6. Construct the network diagram of YTG effective ingredients vs. effective targets

Based on the effective targets dataset of YTG anti-CAD, this study created an association file between the ingredient nodes and the target nodes, and an attribute file of all nodes (Is 1 node belonging to the source node or target node?). Then, the above 2 files were uploaded into the network drawing software Cytascape,[24] the isolated nodes in the network diagram were deleted, the network diagram was constructed and beautified, and the network diagram construction of YTG "Effective Ingredients vs. Effective Targets" was completed.

2.7. PPI networks and core targets

In the form of multiple proteins, the above effective targets were imported into the STRING network platform[25] (https://cn.string-db.org/). After the confidence level being set to the highest level of 0.9, and the orphaned nodes were hidden, the PPI network diagram of YTG was generated using STRING. The PPI data were then downloaded and imported into Cytoscape. Using the plug-in of CytoNCA,[26] this study obtained the 5 network topology parameter scores of each network node (Degree, Eigenvector, LAC, Betweenness and Closeness). Next, the node' data of the above topology parameters were downloaded from Cytoscape, and the core targets of the PPI network were screened by EXCEL with the guidelines: if each topology parameter value of 1 node exceeds the corresponding average value of all nodes, it will be considered as a core target. Subsequently, all core targets passing screening were imported into STRING again to achieve the core target PPI network diagram.

2.8. Enrichment analysis of gene ontology and Kyoto Encyclopedia of Genes and Genomes pathway

The effective targets of YTG were imported into the Metascape[27] (https://metascape.org/) network platform, and enrichment analysis of gene ontology (GO) and Kyoto Encyclopedia of Genes and Genomes (KEGG) pathways was carried out automatically using Metascape. The analysis results were downloaded and arranged, and the data with the top 10 *P*-values were imported into the bioinformatics network platform (https://www.bioinformatics.com.cn/) to visualize them in the form of a bubble chart.

2.9. The analysis of effective ingredients (core ingredients) vs. effective targets (core targets) and participation in signal pathways

Based on the effective target data and the ten main pathways' data of YTG anti-CAD, the YTG network file involving important ingredients, targets and pathways was created using EXCEL. The effective target data were processed as follows: the node of the effective ingredient was listed as the source node, and the node of the effective target was listed as the target node. The data from the ten main pathways were processed as follows: the effective target was listed as the source node, and the pathway was listed as the target node. Based on the data above, a node attribute file was created as follows: the attribute value of each effective ingredient was set to 1, the attribute value of each effective target was set to 2, and the attribute value of each main pathway was set to 3. After the above 2 files were uploaded into Cytoscape, the isolated nodes in the network were deleted, and network diagram was constructed and beautified, and the YTG network diagram of "Effective Ingredients vs. Effective Targets vs. High *P*-value Pathways" was generated. Using similar methods, the YTG network diagram of "Core Ingredients vs. Core Targets vs. Principal Pathways" was also generated.

2.10. Evaluate the affinity between the ligand of ingredient and the receptor of target protein through molecular docking

In this study, the semi-flexible molecular docking mode was adopted, where the receptor target protein was regarded as a rigid body and the ligand small molecule was regarded as a flexible body. First, the 2D structural SDF file of each core ingredient was downloaded from PubChem. Second, the 3D structure with the lowest energy of each core ingredient was generated by the "Chem3D" module of the software Chemoffice,[28] and was saved in the format of mol2. Third, the complete human 3D structure "pdb" format file of each target protein was downloaded from "AlphaFoldDB" data source in the network database of UniProt[29] (https://www.uniprot.org/), and all affiliated subunits and peptide chains, water molecules, and small-molecule ligands in each 3D structure were removed. Fourth, each receptor protein was processed by adding hydrogen atoms and calculating charges using the AutoDocktools software.[30] Then, both the receptor protein processed and its ligand small molecule were converted to "pdpqt" format file, and the docking range was set by the software according to the 3D conformation of the receptor protein. Fifth, AutoDock Vina[31] software was used to carry out molecular docking between the ligand small molecule and the receptor protein 1 by 1, so as to verify the affinity of ingredient and target in the "Core Ingredients vs. Core Targets vs. Pathways" network diagram. Finally, Open-Source software "PyMOL 2.0, LLC"[32] based Python language was used to carry out 3-dimensional visualization of docking results with higher affinity scores.

2.11. Explore the molecule mechanism of YTG in anti-CAD

Combined the target' verification data of platform HIT, "Core Ingredients vs. Core Targets vs. Principal Pathways" network diagram, results of molecular docking between core ingredients and core targets, and some supplementary data obtained by consulting literatures in PubMed and PubChem, the pharmacological mechanism of YTG multimolecular in anti-CAD was explored.

3. Results

3.1. Total ion chromatography

The total ion chromatography (TIC) of YTG in positive ion mode/negative ion mode is shown in Figure 1A and C, and the TIC of blank sample under positive ion mode/negative ion mode was shown in Figure 1B and D.

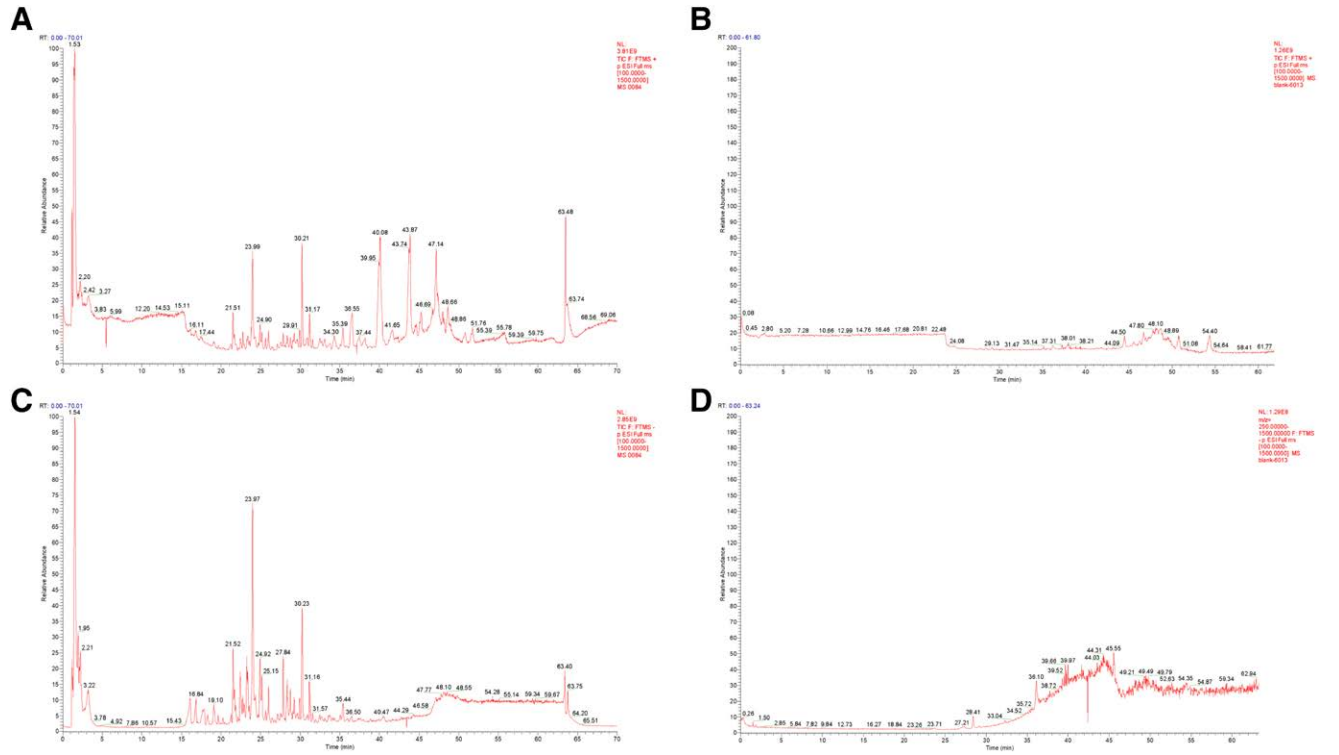

Figure 1. TIC of YTG sample and blank sample. (A) YTG sample in positive ion mode. (B) blank sample in positive ion mode. (C) YTG sample in negative ion mode. (D) blank sample in negative ion mode. TIC is an analytical technique that illustrates the variations in the intensity of all ion signals detected over a specified time frame. TIC aggregates the intensities of all ions at each retention time, thereby facilitating the identification and quantification of various components in complex samples. TIC = total ion chromatography, YTG = Yixin Tongmai Granules.

3.2. Active ingredients collection of YTG

As shown in Table 2, 131 ingredients were identified using Compound Discoverer 3.3. The data of violations (Lipinski(L), Ghose(G), Veber(V), Egan(E), and Muegge(M)), and bioavailability score were obtained from SwissADME. Among the above 131 ingredients, there were 33 whose relative content in the drug exceeded 0.5%. In addition, there were 18 ingredients among the 33 ingredients, that had passed the ADME screening by the SwissADME platform. In terms of content, they are tanshinone IIA, cryptotanshinone, dihydrotanshinone I, citric acid, caffeic acid, danshensu, protocatechualdehyde, liquiritigenin, ononin, liquiritin, formononetin, calycosin, licochalcone A, calycosin-7-o-beta-D-glucoside, licochalcone B, nicotinic acid, ligustilide, and glabrone.

3.3. Targets collection and screening of YTG

This study then used HIT to search for the targets of the 18 active ingredients individually, to obtain targets supported by documentary evidence. After retrieval, 12 ingredients with HIT targets were identified: tanshinone IIA, cryptotanshinone, dihydrotanshinone I, citric acid, caffeic acid, danshensu, protocatechualdehyde, liquiritin, formononetin, calycosin, nicotinic acid, and ligustilide. After removing the target duplicates, 96 strong HIT targets were obtained. As a supplement to HIT retrieval, the potential targets of the above 18 ingredients were predicted by SwissTargetPrediction based on a probability threshold of 0.5, and there were 9 ingredients with targets greater than or equal to the threshold: tanshinone IIA, cryptotanshinone, dihydrotanshinone I, caffeic acid, liquiritigenin, ononin, formononetin, calycosin-7-o-beta-D-glucoside, and nicotinic acid. Thus, 26 high probability targets were obtained after removing the duplicates. Then, the targets of the 2 platforms were merged, and 116 high-reliability targets of YTG were obtained, involving 15 active ingredients.

3.4. Collection of CAD targets

10,750 disease targets were collected from GeneCards with the Keyword of "Coronary artery disease" as the keyword, while 9962 disease targets were collected from GeneCards with the keyword of "Coronary heart disease" as the key word. After removing duplicates, 11,050 disease targets remained.

3.5. Finding intersection of YTG high-reliability drug targets and CAD-related targets, and mapping the effective ingredients and the effective targets

After the data on high-reliability YTG drug targets and CAD-related targets were imported into Venny 2.1, 96 intersection targets (effective targets shared by drug and disease) were obtained, and the generated Venn diagram is shown in Figure 2A. Based on the 96 effective targets from the intersection (20 drug targets unrelated to CAD were removed), the 14 effective ingredients of YTG were associated; thus, the network diagram of YTG "Effective Ingredients vs. Effective Targets" was generated using Cytoscape, as shown in Figure 2B. The chemical structural formulas of the 14 effective ingredients downloaded from PubChem are shown in Figure 3.

3.6. Construction of PPI network

Then, the 96 effective targets were imported into STRING in the form of multiple proteins, and the PPI network of YTG targets was obtained, with a total of 260 interaction edges, as shown in Figure 4A. Subsequently, the network data downloaded from STRING were imported into Cytoscape, and the CytoNCA plug-in was used to calculate the 5 network topology parameter scores (Degree, Eigenvector, LAC, Betweenness, and Closeness) of each node in the PPI network. The targets, whose 5 scores all exceeded the average values (6.441558442,

Table 2

Information of ingredients identified in YTG.

Molecule	Formula	MW	Lipinski #violations	Ghose #violations	Veber #violations	Egan #violations	Muegge #violations	Bioavailability Score	Matching score	Peak area	Relative content(%)
Tanshinone IIA	$C_{19}H_{18}O_3$	294.34	0	0	0	0	0	0.55	89.1	10,974,600,332	13.61
Cryptotanshinone	$C_{19}H_{20}O_3$	296.36	0	0	0	0	0	0.85	86	10,767,425,881	13.353
Diammonium glycyrrhizinate	$C_{42}H_{68}N_2O_{16}$	856.99	3	3	1	1	5	0.11	93	5,598,303,566	6.942
Dihydrotanshinone I	$C_{18}H_{14}O_3$	278.3	0	0	0	0	0	0.85	90.7	3,793,493,283	4.704
Salvianolic acid A	$C_{26}H_{22}O_{10}$	494.45	1	2	1	1	2	0.11	93.4	3,609,089,378	4.476
18 β-Glycyrrhetintic Acid	$C_{30}H_{46}O_4$	470.68	1	3	0	1	1	0.85	85.8	3,594,042,375	4.457
Citric acid	$C_6H_8O_7$	192.12	0	2	0	1	1	0.56	91	2,999,815,813	3.72
Caffeic acid	$C_9H_8O_4$	180.16	0	0	0	0	1	0.56	83.3	2,854,135,133	3.539
Danshensu	$C_9H_{10}O_5$	198.17	0	0	0	0	1	0.56	89.9	2,636,210,395	3.269
Sucrose	$C_{12}H_{22}O_{11}$	342.3	2	1	1	1	4	0.17	95.2	2,614,709,110	3.242
Liguiritigenin-7-O-D-apiosyl-4'-O-D-glucoside	$C_{26}H_{30}O_{13}$	550.51	3	2	1	1	3	0.17	91.5	2,447,522,138	3.035
Protocatechualdehyde	$C_7H_6O_3$	138.12	0	3	0	0	1	0.55	92.4	2,044,959,301	2.536
Liquiritigenin	$C_{15}H_{12}O_4$	256.25	0	0	0	0	0	0.55	91.1	1,838,794,890	2.28
Glycyrrhizic acid	$C_{42}H_{62}O_{16}$	822.93	3	3	1	1	4	0.11	92.6	1,499,782,248	1.86
Stachyose	$C_{24}H_{42}O_{21}$	666.58	3	4	2	1	5	0.17	91	1,371,967,868	1.701
Ononin	$C_{22}H_{22}O_9$	430.4	0	0	0	1	0	0.55	88.3	1,309,110,081	1.623
Cryptochlorogenic acid	$C_{16}H_{18}O_9$	354.31	1	1	1	1	2	0.11	93.4	965,277,155.9	1.197
Lithospermic acid	$C_{27}H_{22}O_{12}$	538.46	3	2	1	1	3	0.11	94.3	915,765,257.6	1.136
Liquiritin	$C_{21}H_{22}O_9$	418.39	0	0	1	1	0	0.55	80.5	874,373,661.8	1.084
Harpagide	$C_{15}H_{24}O_{10}$	364.35	1	1	1	1	3	0.55	95.6	802,683,620.4	0.995
Formononetin	$C_{16}H_{12}O_4$	268.26	0	0	0	0	0	0.55	89.3	793,784,385.5	0.984
Harpagoside	$C_{24}H_{30}O_{11}$	494.49	2	2	1	1	3	0.17	75.4	777,749,714.9	0.964
Angoroside C	$C_{36}H_{48}O_{19}$	784.75	3	4	2	1	4	0.17	94.9	777,701,944.9	0.964
Calycosin	$C_{16}H_{12}O_5$	284.26	0	0	0	0	0	0.55	88.4	703,538,274.7	0.872
Licochalcone A	$C_{21}H_{22}O_4$	338.4	0	0	0	0	0	0.55	91	698,284,820.8	0.866
Astragaloside IV	$C_{41}H_{68}O_{14}$	784.97	3	3	1	1	5	0.17	75.7	551,403,345.8	0.684
Calycosin-7-O-β-D-glucoside	$C_{22}H_{22}O_{10}$	446.4	0	0	1	1	1	0.55	87.4	523,774,346.4	0.65
Licochalcone B	$C_{16}H_{14}O_5$	286.28	0	0	0	0	0	0.55	90.1	513,057,715.4	0.636
Manninotriose	$C_{18}H_{32}O_{16}$	504.44	3	2	2	1	4	0.17	84	478,406,864	0.593
Nicotinic acid	$C_6H_5NO_2$	123.11	0	3	0	0	1	0.85	84.1	469,706,054.9	0.582
Ligustilide	$C_{12}H_{14}O_2$	190.24	0	0	0	0	1	0.55	84.6	466,621,795.5	0.579
Gypenoside XVII	$C_{48}H_{82}O_{18}$	947.15	3	3	2	1	4	0.17	85.3	436,558,648.2	0.541
Glabrone	$C_{20}H_{16}O_5$	336.34	0	0	0	0	0	0.55	87.2	427,949,972.5	0.531
1,3-Dicaffeoylquinic acid	$C_{25}H_{24}O_{12}$	516.45	3	1	1	1	3	0.11	92.5	408,403,496.4	0.506
Salvianolic acid C	$C_{26}H_{20}O_{10}$	492.43	1	1	1	1	2	0.11	79.5	394,532,764.9	0.489
Quinic acid	$C_7H_{12}O_6$	192.17	0	1	0	0	2	0.56	83.4	353,406,509.6	0.438
3-Butylidenephthalide	$C_{12}H_{12}O_2$	188.22	0	0	0	0	1	0.55	86	318,275,490.2	0.395
Ginsenoside Rc	$C_{53}H_{90}O_{22}$	1079.27	3	4	2	1	6	0.17	82.5	316,754,478	0.393
Ginsenoside Rg1	$C_{42}H_{72}O_{14}$	801.01	3	3	1	1	4	0.17	91.3	305,327,301.1	0.379
Sophocarpine	$C_{15}H_{22}N_2O$	246.35	0	0	0	0	0	0.55	86.1	295,171,668.5	0.366
4-Methoxysalicylic acid	$C_8H_8O_4$	168.15	0	0	0	0	1	0.85	78.7	289,867,893	0.359
Trigonelline HCl	$C_7H_8ClNO_2$	173.6	0	2	0	0	1	0.85	86.8	279,140,505.6	0.346
Lupenone	$C_{30}H_{48}O$	424.7	1	3	0	1	2	0.55	86.4	276,032,015.3	0.342
Licoflavone A	$C_{20}H_{18}O_4$	322.35	0	0	0	0	1	0.55	87.2	274,257,890.5	0.34
Ginsenoside Ro	$C_{48}H_{76}O_{19}$	957.11	3	3	1	1	5	0.11	84.8	267,720,650.3	0.332
Isoacteoside	$C_{29}H_{36}O_{15}$	624.59	3	4	2	1	4	0.17	92.6	259,324,579.5	0.322
5-Hydroxymethylfurfural	$C_6H_6O_3$	126.11	0	3	0	0	1	0.55	79.7	258,946,529.9	0.321
Ferulic acid	$C_{10}H_{10}O_4$	194.18	0	0	0	0	1	0.85	83.6	244,553,461.8	0.303
Cinnamic acid	$C_9H_8O_2$	148.16	0	2	0	0	1	0.85	72.7	230,280,621.8	0.286
Curcumenol	$C_{15}H_{22}O_2$	234.33	0	0	0	0	0	0.55	89.2	221,828,586.8	0.275
Senkyunolide A	$C_{12}H_{16}O_2$	192.25	0	0	0	0	1	0.55	90.2	221,549,955.9	0.275
Paeonol	$C_9H_{10}O_3$	166.17	0	0	0	0	1	0.55	72.6	220,747,180.2	0.274
Quillaic acid	$C_{30}H_{46}O_5$	486.68	0	3	0	0	1	0.56	75.1	200,265,590.2	0.248
Ginsenoside Rb1	$C_{54}H_{92}O_{23}$	1109.29	3	4	2	1	6	0.17	87.7	192,173,341.9	0.238
Azelaic acid	$C_9H_{16}O_4$	188.22	0	0	0	0	1	0.85	79.7	191,305,426.5	0.237
Daidzein	$C_{15}H_{10}O_4$	254.24	0	0	0	0	0	0.55	75.5	189,869,294.3	0.235
Isoliquiritin	$C_{21}H_{22}O_9$	418.39	1	0	1	1	2	0.55	89.8	173,119,557.7	0.215
Retrochalcone	$C_{16}H_{14}O_4$	270.28	0	0	0	0	0	0.55	87.6	155,149,983.6	0.192
Ginsenoside Rf	$C_{42}H_{72}O_{14}$	801.01	3	3	1	1	4	0.17	91.1	154,564,833.7	0.192
Dehydronuciferine	$C_{19}H_{19}NO_2$	293.36	0	0	0	0	0	0.55	80.2	145,265,237.4	0.18
Maltopentaose	$C_{30}H_{52}O_{26}$	828.72	3	4	2	1	6	0.17	91.9	135,706,907.7	0.168

(*Continued*)

Table 2

(*Continued*)

Molecule	Formula	MW	Lipinski #violations	Ghose #violations	Veber #violations	Egan #violations	Muegge #violations	Bioavailability Score	Matching score	Peak area	Relative content(%)
Matrine	$C_{15}H_{24}N_2O$	248.36	0	0	0	0	0	0.55	70.2	122,580,612.2	0.152
Isoliquiritigenin	$C_{15}H_{12}O_4$	256.25	0	0	0	0	0	0.55	89.9	117,504,872.3	0.146
20 (R)-Ginsenoside Rg2	$C_{42}H_{72}O_{13}$	785.01	3	3	1	1	4	0.17	91.4	115,331,892.1	0.143
Uridine	$C_9H_{12}N_2O_6$	244.2	0	1	0	0	0	0.55	91	114,214,198.9	0.142
Ginsenoside Rg3	$C_{42}H_{72}O_{13}$	785.01	3	3	1	1	4	0.17	90.7	100,763,787.8	0.125
Forsythoside E	$C_{20}H_{30}O_{12}$	462.45	2	1	1	1	4	0.17	75.5	94,556,085.99	0.117
α-Linolenic acid	$C_{18}H_{30}O_2$	278.43	1	1	1	0	1	0.85	76.5	87,894,988.82	0.109
Salicylic acid	$C_7H_6O_3$	138.12	0	3	0	0	1	0.85	82.6	82,036,868.37	0.102
Ginsenoside Rb3	$C_{53}H_{90}O_{22}$	1079.27	3	4	2	1	5	0.17	81.2	73,197,120.25	0.091
Isochlorogenic acid B	$C_{25}H_{24}O_{12}$	516.45	3	1	1	1	3	0.11	91.5	71,683,409.53	0.089
Levistilide A	$C_{24}H_{28}O_4$	380.48	1	0	0	0	0	0.55	80.7	70,142,657.41	0.087
Baicalin	$C_{21}H_{18}O_{11}$	446.36	2	0	1	1	3	0.11	86.7	67,590,781.07	0.084
Nicotinamide	$C_6H_6N_2O$	122.12	0	3	0	0	1	0.55	77.6	66,691,449.1	0.083
Isomucronulatol 7-O-glucoside	$C_{23}H_{28}O_{10}$	464.46	0	0	1	1	0	0.55	89.2	65,752,468.1	0.082
Ethyl caffeate	$C_{11}H_{12}O_4$	208.21	0	0	0	0	0	0.55	83.4	64,696,561.83	0.08
Kanzonol C	$C_{25}H_{28}O_4$	392.49	0	1	0	0	1	0.55	74.2	58,579,795.93	0.073
Ginsenoside F2	$C_{42}H_{72}O_{13}$	785.01	3	3	1	1	4	0.17	92.5	52,241,956.51	0.065
Glabrolide	$C_{30}H_{44}O_4$	468.67	1	3	0	0	1	0.55	76.1	49,236,048.06	0.061
20 (R)-Notoginsenoside R2	$C_{41}H_{70}O_{13}$	770.99	3	3	1	1	4	0.17	89.2	48,030,014.76	0.06
4-Methyl-6,7-dihydroxycoumarin	$C_{10}H_8O_4$	192.17	0	0	0	0	1	0.55	80.4	43,212,534.31	0.054
Methyl rosmarinate	$C_{19}H_{18}O_8$	374.34	0	0	0	1	0	0.55	74.2	42,763,145.85	0.053
Xanthotoxol	$C_{11}H_6O_4$	202.16	0	0	0	0	0	0.55	80.6	40,163,973.84	0.05
Genistein	$C_{15}H_{10}O_5$	270.24	0	0	0	0	0	0.55	74.9	40,001,909.67	0.05
Ginsenoside Rd	$C_{48}H_{82}O_{18}$	947.15	3	3	2	1	4	0.17	81.6	36,362,501.6	0.045
Arglabin	$C_{15}H_{18}O_3$	246.3	0	0	0	0	0	0.55	73.5	34,098,603.41	0.042
2-Hydroxy-4-methoxybenzaldehyde	$C_8H_8O_3$	152.15	0	2	0	0	1	0.55	76.6	32,690,117.35	0.041
Ferulaldehyde	$C_{10}H_{10}O_3$	178.18	0	0	0	0	1	0.55	74	32,551,076.3	0.04
Rosmarinic acid	$C_{18}H_{16}O_8$	360.31	0	0	1	1	0	0.56	76.4	30,278,046.18	0.038
Protocatechuic acid	$C_7H_6O_4$	154.12	0	3	0	0	1	0.56	81.6	28,957,403.92	0.036
6''-O-Acetylglycitin	$C_{24}H_{24}O_{11}$	488.44	1	1	1	1	2	0.55	82.1	28,769,898.74	0.036
Ursonic acid	$C_{30}H_{46}O_3$	454.68	1	3	0	1	1	0.85	86.7	26,790,855.03	0.033
Aucubin	$C_{15}H_{22}O_9$	346.33	1	1	1	1	2	0.55	80	26,444,864.98	0.033
Esculetin	$C_9H_6O_4$	178.14	0	1	0	0	1	0.55	83.9	25,757,927.3	0.032
1-Caffeoylquinic acid	$C_{16}H_{18}O_9$	354.31	1	1	1	1	2	0.11	84.6	24,566,609.59	0.03
8-Methoxypsoralen	$C_{12}H_8O_4$	216.19	0	0	0	0	0	0.55	77	23,688,959	0.029
L-Tryptophan	$C_{11}H_{12}N_2O_2$	204.23	0	0	0	0	0	0.55	83.7	22,804,727.05	0.028
Wilforlide A	$C_{30}H_{46}O_3$	454.68	1	3	0	1	1	0.55	74.3	22,639,477.99	0.028
Icaritin	$C_{21}H_{20}O_6$	368.38	0	0	0	0	0	0.55	73.6	21,830,670.95	0.027
p-Coumaric acid	$C_9H_8O_3$	164.16	0	0	0	0	1	0.85	79.3	21,479,898.08	0.027
Skimmin	$C_{15}H_{16}O_8$	324.28	0	1	0	0	0	0.55	74.2	19,810,114.34	0.025
Diosmetin-7-O-β-D-glucopyranoside	$C_{22}H_{22}O_{11}$	462.4	2	0	1	1	3	0.17	85.8	19,636,800.57	0.024
Scopoletin	$C_{10}H_8O_4$	192.17	0	0	0	0	1	0.55	74.7	19,263,377.22	0.024
Methylnissolin-3-O-glucoside	$C_{23}H_{26}O_{10}$	462.45	0	0	0	1	0	0.55	84.1	19,082,019.97	0.024
Linarin	$C_{28}H_{32}O_{14}$	592.55	3	4	1	1	3	0.17	88.6	18,995,348.21	0.024
Medicarpin	$C_{16}H_{14}O_4$	270.28	0	0	0	0	0	0.55	71.3	18,835,151.4	0.023
Sibiricose A5	$C_{22}H_{30}O_{14}$	518.47	3	2	1	1	3	0.17	87.7	17,937,282.7	0.022
Roburic acid	$C_{30}H_{48}O_2$	440.7	1	3	0	1	1	0.85	70.6	17,250,834.32	0.021
Benzoic acid	$C_7H_6O_2$	122.12	0	3	0	0	1	0.85	83.9	16,193,680.42	0.02
Chikusetsu saponin IVa	$C_{42}H_{66}O_{14}$	794.97	3	3	1	1	4	0.11	70.8	16,069,487.03	0.02
Nobiletin	$C_{21}H_{22}O_8$	402.39	0	0	0	0	0	0.55	86.1	15,446,266.16	0.019
Dipotassium glycyrrhizinate	$C_{42}H_{60}K_2O_{16}$	899.11	3	4	1	1	4	0.11	83.8	15,320,079.34	0.019
Hydroxygenkwanin	$C_{16}H_{12}O_6$	300.26	0	0	0	0	0	0.55	74.4	15,217,351.2	0.019
Gentisic acid	$C_7H_6O_4$	154.12	0	3	0	0	1	0.56	87	15,168,495.46	0.019
Artemisinic acid	$C_{15}H_{22}O_2$	234.33	0	0	0	0	0	0.85	75	14,710,707.85	0.018
Glabridin	$C_{20}H_{20}O_4$	324.37	0	0	0	0	0	0.55	79.4	13,502,797.1	0.017
Gallic acid	$C_7H_6O_5$	170.12	0	2	0	0	1	0.56	86.6	12,458,385.95	0.015
Isoalantolactone	$C_{15}H_{20}O_2$	232.32	0	0	0	0	0	0.55	79.7	12,205,208.16	0.015

(*Continued*)

Table 2

(*Continued*)

Molecule	Formula	MW	Lipinski #violations	Ghose #violations	Veber #violations	Egan #violations	Muegge #violations	Bioavailability Score	Matching score	Peak area	Relative content(%)
Apigenin-7-O-β-D-glucoside	$C_{21}H_{20}O_{10}$	432.38	1	0	1	1	2	0.55	84.4	12,102,768.85	0.015
Calcium pantothenate	$C_{18}H_{32}CaN_2O_{10}$	476.53	2	1	2	1	3	0.17	81.5	11,695,334.26	0.015
Naringenin chalcone	$C_{15}H_{12}O_5$	272.25	0	0	0	0	0	0.55	77.8	11,293,192.77	0.014
Notoginsenoside	$C_{47}H_{80}O_{17}$	917.13	3	3	2	1	4	0.17	93.7	11,265,441.21	0.014
Wogonoside	$C_{22}H_{20}O_{11}$	460.39	1	0	1	1	2	0.11	75.7	10,932,389.62	0.014
Hesperidin	$C_{28}H_{34}O_{15}$	610.56	3	4	1	1	4	0.17	90.7	10,215,955.59	0.013
Ethyl 3,4-dihydroxybenzoate	$C_9H_{10}O_4$	182.17	0	0	0	0	1	0.55	78.5	10,006,657.22	0.012
Tectoridin	$C_{22}H_{22}O_{11}$	462.4	2	0	1	1	3	0.17	75.4	8,728,105.688	0.011
Isoschaftoside	$C_{26}H_{28}O_{14}$	564.49	3	3	1	1	4	0.17	75.7	5,892,194.89	0.007
Pyrogallol	$C_6H_6O_3$	126.11	0	3	0	0	1	0.55	83.9	5,830,736.56	0.007
Purpureaside C	$C_{35}H_{46}O_{20}$	786.73	3	4	2	1	5	0.17	90.6	4,954,673.445	0.006
Ginsenoside F1	$C_{36}H_{62}O_9$	638.87	2	3	1	1	3	0.17	83.5	4,173,622.912	0.005
Isobavachin	$C_{20}H_{20}O_4$	324.37	0	0	0	0	0	0.55	70.9	2,230,608.728	0.003

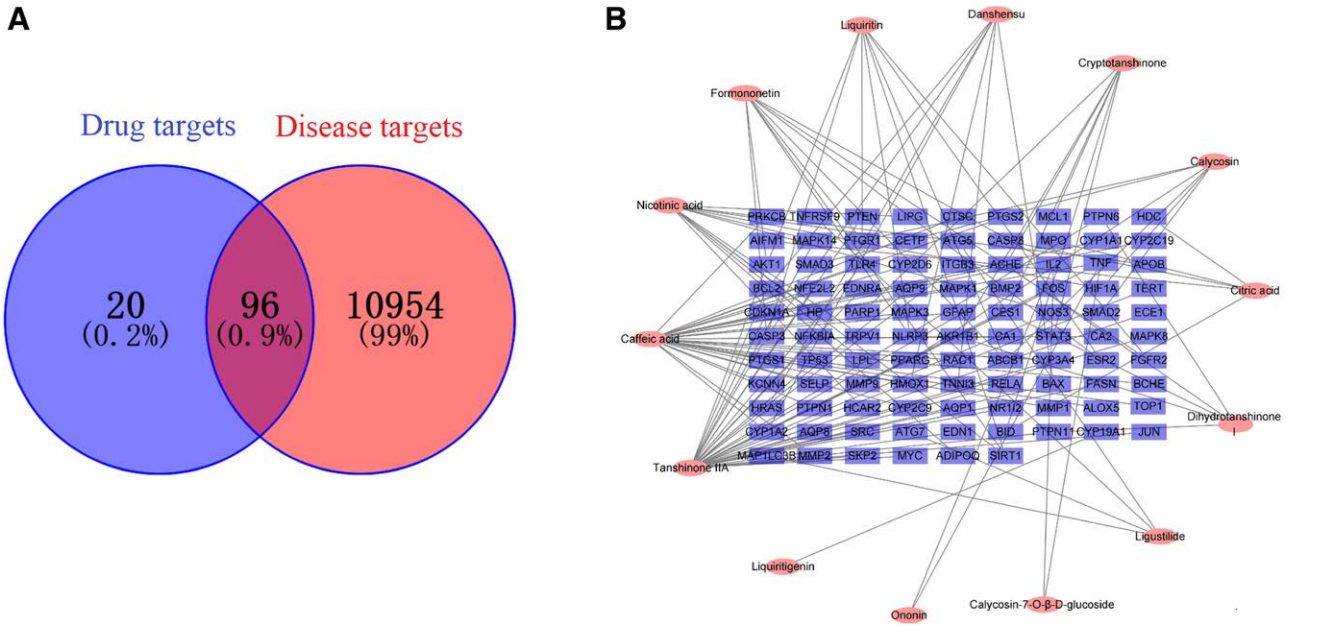

Figure 2. The intersection of YTG high-reliability targets and CAD-related targets, and mapping diagram of "Effective ingredients vs. Effective target." (A) Venn diagram of YTG drug targets and CAD-related targets. (B) Network diagram of YTG "Effective Ingredients vs. Effective Targets." A Venn diagram is a graphical representation that illustrates the relationships among different sets of items. It typically consists of overlapping circles, with each circle representing a distinct set. The overlapping areas illustrate the common elements shared between some different sets. The ingredient-target network diagram is a graphical tool used to illustrate the interactions between drug ingredients and their targets. This type of diagram assists researchers in understanding the mechanisms of drug action, particularly the multi-ingredient and multi-target characteristics of TCM formulations. CAD = coronary artery disease, TCM = traditional Chinese medicine, YTG = Yixin Tongmai Granules.

0.073029977, 2.578057501, 160.9610397, 0.336205355) of all PPI network nodes were regarded as core targets. The core target proteins obtained via the above analysis were TP53, STAT3, transcription factor Jun (JUN), MAPK3, MAPK1, AKT1, SRC, MYC, BCL2, transcription factor p65 (RELA), TNF, and ESR2 (Table 3). At last, the 12 core targets were imported into STRING again to acquire the PPI network diagram of the 12 core targets, and the PPI diagram network between them was shown in Figure 4B. If the 12 targets were graded again using the same analysis method (the average values of the 5 topology parameters were 17.25, 0.226355519, 6.346420192, 509.7143875, and 0.440291293), the most important target, TP53, was obtained.

3.7. GO and KEGG pathway enrichment analysis

The 96 effective targets of YTG for anti-CAD were imported into Metascape for GO analysis (including GO biological process, GO cell component, and GO molecular function) and KEGG pathway analysis. The analyzed data were then downloaded (*P*-value, enrichment score of each item, and number of effective target genes participating in the item). Subsequently, the top 10 items' data of GO analysis and KEGG pathway analysis were imported into the bioinformatics platform for visualization in the form of a bar chart (Fig. 5A) and bubble chart (Fig. 5B).

The top 10 pathways with higher *P*-values were classified according to their association as follows: arteriosclerosis

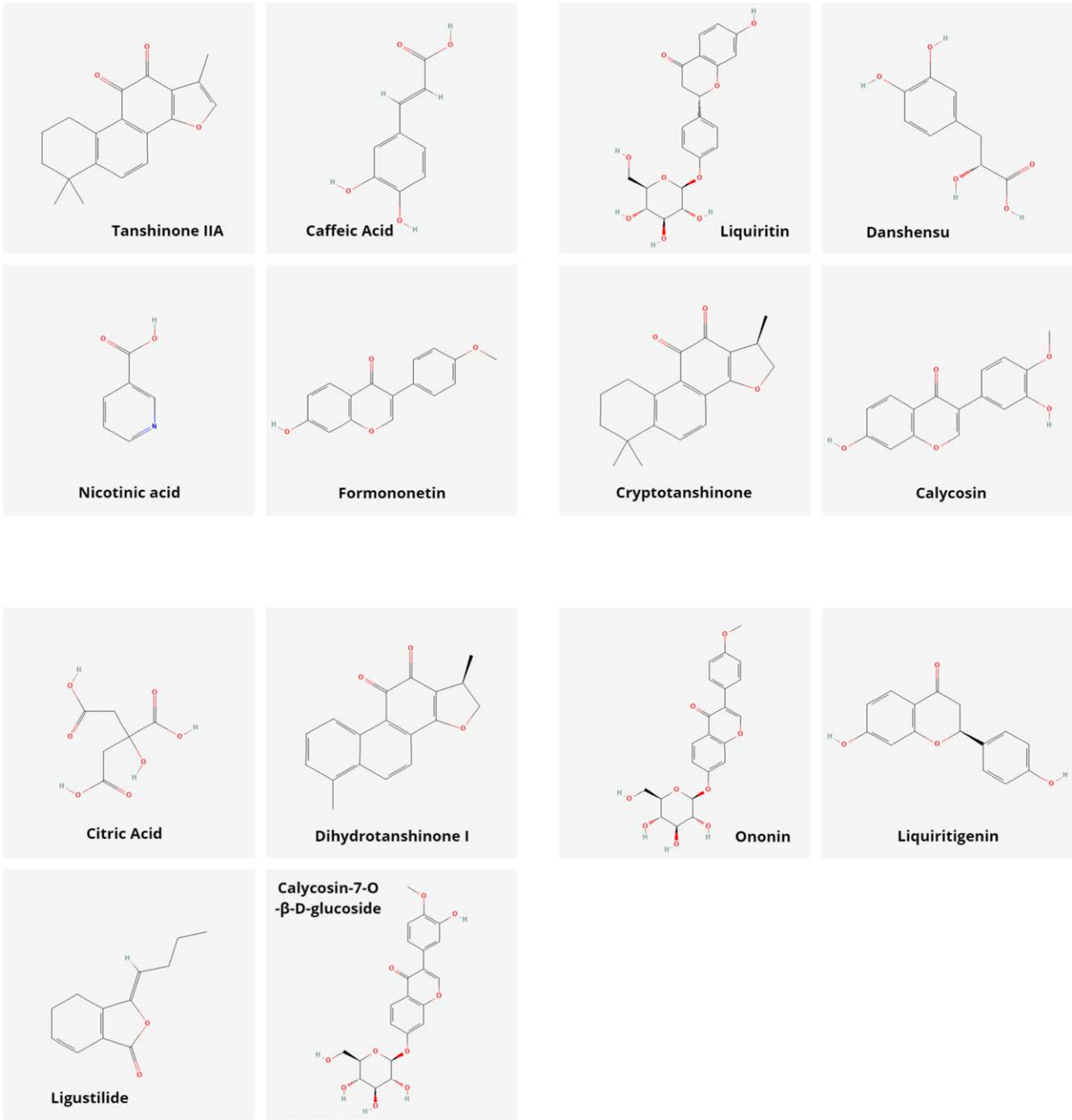

Figure 3. The chemical structural formulas of 14 effective ingredients. The figure illustrates the 2D chemical structures of these organic molecules, which primarily consist of the elements carbon (C), hydrogen (H), and oxygen (O).

(hsa05417), cancer (hsa05200, hsa05205, hsa01522, and hsa05210), viruses (hsa05161, hsa05167, and hsa05163), diabetes (hsa04933), and apoptosis (hsa04210). Arteriosclerosis refers to the thickening and hardening of the arterial wall, loss of elasticity, and narrowing of the lumen. The pathology of CAD is the occurrence of atherosclerosis in the coronary arteries, that is, atherosclerosis is the underlying cause of CAD.[33] Atherosclerosis is a chronic inflammatory disease characterized by narrowing of arteries due to lipid-rich plaques (hsa05417) in the arterial wall.[34] Several other pathways are also associated with CAD. Li et al found that CAD is an independent risk factor for cancer (hsa05200) and vice versa, and digestive, respiratory, and urogenital cancers are susceptible to CAD.[35] Some microbial infections have been shown to induce CAD.[36] Du et al confirmed that human cytomegalovirus infection (hsa05163) is closely associated with CAD.[37] However, most microbial infections are not related to CAD. According to a meta-analysis of Wijarnpreecha et al, HBV infection (hsa05161) was excluded as a risk factor for CAD.[38] T2DM is also a major risk factor for CAD,[39] and patients with T2DM tend to develop macrovascular and microvascular complications (hsa04933). Cell apoptosis (hsa04210) is inevitably involved in the pathogenesis, development, and prognosis of CAD.[40]

According to Metascape enrichment analysis of the effective targets, the pathway of "Lipid and Atherosclerosis" (hsa05417) was most significant in *P*-value, with LogP (the logarithm to base 10 of *P*-value) of –42.6. The effective targets involved in this pathway are AKT1, APOB, BAX, BCL2, BID, CASP3, CASP8, CYP1A1, CYP2C9, FOS, HRAS, JUN, MAPK1, MAPK14,

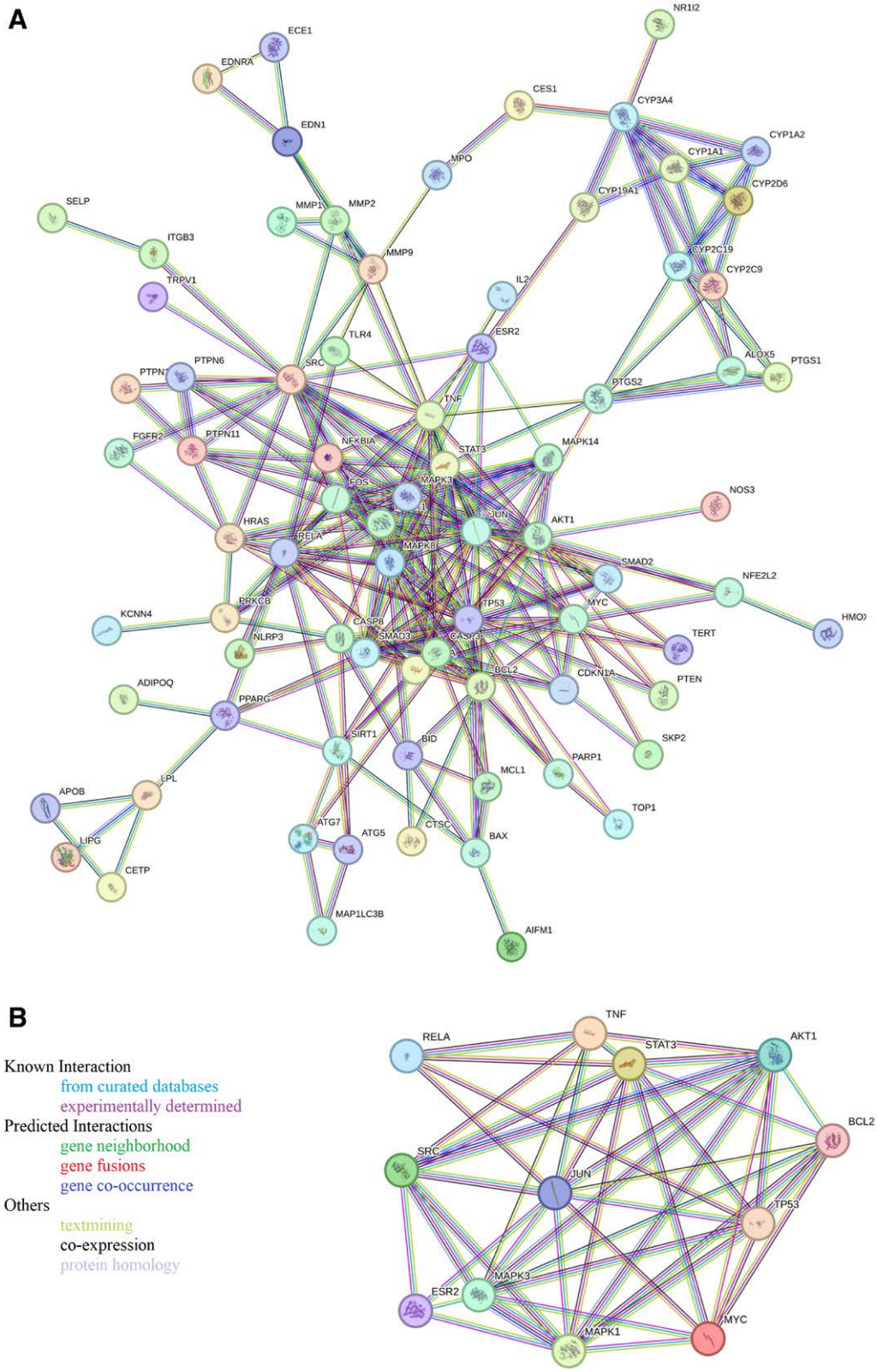

Figure 4. The PPI network diagram of effective targets and core targets of YTG. (A) PPI network diagram of effective targets, (B) PPI network diagram of core targets. A PPI network diagram is a graphical representation used to visualize the interactions between proteins within a biological system. These interactions include known interactions (derived from curated or experimentally determined sources), predicted interactions (such as gene neighborhood, gene fusions, or gene co-occurrence), and other types (such as text mining, co-expression, or protein homology). PPI = protein–protein interaction, YTG = Yixin Tongmai Granules.

MAPK3, MAPK8, MMP1, MMP9, NFE2L2, NFKBIA, NLRP3, NOS3, PPARG, RAC1, RELA, SELP, SRC, STAT3, TLR4, TNF, and TP53, and accounted for 32.29% of the total effective targets. Among them, the proteins of AKT1, BCL2, JUN, MAPK1, MAPK3, RELA, SRC, STAT3, TNF, and TP53 were the core targets, and accounted for 83.33% of the total

Table 3

PPI network topology scores of ten core targets of YTG.

Target	Degree	Eigenvector	LAC	Betweenness	Closeness
TP53	29	0.3198544	6.8965516	1606.6608	0.5
JUN	20	0.2897593	8.8	346.37604	0.46060607
MAPK3	19	0.26850638	7.7894735	251.2178	0.45238096
MAPK1	19	0.2760761	8.421053	222.32639	0.44705883
AKT1	19	0.25926083	7.1578946	400.00418	0.44186047
SRC	18	0.1867733	4.4444447	936.0713	0.42696628
STAT3	17	0.24660847	7.1764708	596.63916	0.47204968
MYC	16	0.22965252	7.125	185.30759	0.4108108
BCL2	16	0.21626037	6	285.85046	0.41758242
RELA	13	0.16079764	4.769231	322.12473	0.4198895
TNF	13	0.14109343	3.0769231	634.2787	0.45238096
ESR2	8	0.12162349	4.5	329.7155	0.38190955

JUN = transcription factor Jun, MAPK1 = MAP kinase-activated protein kinase 1, MAPK3 = MAP kinase-activated protein kinase 3, MYC = myelocytomatosis, PPI = protein–protein interaction, RELA = transcription factor p65, SRC = c-Src, STAT3 = signal transducer and activator of transcription 3, TNF = tumor necrosis factor, TP53 = tumor protein 53.

core targets. the pathway of "Pathways in cancer" (hsa05200) was second most significant in *P*-value, with LogP of −42.42. The effective targets involved in this pathway accounted for 40.63% of the total effective targets. Among them, the proteins of AKT1, BCL2, ESR2, JUN, MAPK1, MAPK3, MYC, RELA, STAT3, and TP53 were the core targets, and accounted for 83.33% of the total core targets. The number of the effective targets in this pathway also appearing in pathway of "Lipid and Atherosclerosis" was 20, accounting for 51.28% of the total effective targets in "Pathways in cancer." The pathway of "AGE-RAGE signaling pathway in diabetic complications" (hsa04933) ranked the forth, whose LogP value is −30.26. The effective targets involved in the pathway accounted for 20.83% of the total. Among them, the core targets involved are AKT1, BCL2, JUN, MAPK1, MAPK3, RELA, STAT3, and TNF, and accounted for 66.67% of the total core targets. The pathway of "Apoptosis" (hsa04210) ranked the sixth, whose LogP value is −27.38. The effective targets accounted for 20.83% of the total. Among them, the core targets involved are AKT1, BCL2, JUN, MAPK1, MAPK3, RELA, TNF and TP53, and accounted for 66.67% of the total. The pathway of "Human cytomegalovirus infection" (hsa05163) ranked the ninth, whose LogP value is −24.44. The effective targets accounted for 21.88% of the total. Among them, the core targets involved are AKT1, MYC, MAPK1, MAPK3, RELA, SRC, STAT3, TNF and TP53, and accounted for 75% of the total. After removing the second item (Hepatitis B, hsa05161), the top 3 pathways in *P*-value are hsa05417, hsa05200 and hsa04933 successively. This study named these 3 pathways as principal pathways, and the diagrams of the 3 pathways which reflect the role of genes involved in pathways can be found in Supplementary Data 1, Supplemental Digital Content, http://links.lww.com/MD/O414. Then, the associations of between ingredients, targets and pathways were imported into the Cytoscape, and the network diagram of "Effective Ingredients vs. Effective Targets vs. High *P*-value Pathways" was thus built, as shown in Figure 6A. Further, the network diagram of "Core Ingredients vs. Core Targets vs. Principal Pathways" was also obtained, as shown in Figure 6B.

3.8. The affinities were verified molecular docking

In this study, according to Figure 6B, as small-molecule ligands, the 2D structure files of 7 core ingredients of YTG were downloaded from PubChem, and were processed with the lowest energy by Chem3D. As macromolecular receptors, the 3D structure PDB files of the 12 core targets of YTG were downloaded from "AlphaFoldDB" data source of UniProt. Then, AutoDocktools was used in the pretreatment before molecular docking, and AutoDock Vina was used to carry out molecular docking 1 by 1 between the core ingredients, and their core targets associated. If the docking score is less than or equal to −5.0 kcal/mol, it is generally agreed that there is good affinity between the ligand and the receptor. Further, if the docking score is less than or equal to −7.0 kcal/mol, it is generally agreed that there is very good affinity between them. The 3D docking visualizing simulation diagrams generated by PyMOL, between ingredients and targets, as shown in Figure 7. Most of the docking scores in this study are below −5.0 kcal/mol, of which the best, i.e. docking between Tanshinone IIA and AKT1 is −8.8 kcal/mol.

3.9. Multi-source data integration

To evaluate the interactions between the core ingredients and the core targets of YTG in the treatment of CAD, the HIT grading data with literature support and the affinity data of molecular docking between ligands and targets are summarized in Table 4. In this table, the HIT grading levels (A, B, C, or N/A) represent the confidence indicators of the targets. Their meanings are as follows: "A" represents "direct inhibition/activation"; "B" represents "indirect inhibition/activation," "enzyme substate" and "enzyme product"; "C" represents "up/down regulation" and "other"; "N/A" represents no literature record (predicted by SwissTargetPrediction with higher probability). The latest proof can be found in the recommended literature on the HIT. For example, the thesis of Du[41] stated that cryptotanshinone is an effective inhibitor of STAT3.

4. Discussion

4.1. Literatures related to core targets

STAT3 belongs to the STAT protein family, responds to some cytokines and growth factors, and acts as a transcriptional factor for genes related to cell growth, differentiation, and survival.[42] STAT3 is activated by phosphorylation of the site Tyr^{705}. Sustained activation of STAT3 leads to the overexpression of adhesion molecules ICAM1 and VCAM1.[43] Abnormally increased adhesion molecules lead to inflammation and accelerate endothelial cell dysfunction, exacerbating atherosclerosis.[44] Inhibition of STAT3 activity by decreasing STAT3 phosphorylation prevents inflammation and monocyte-to-macrophage differentiation, 2 factors that accentuating atherosclerosis.[45] The abnormal proliferation of VSMCs can promote plaque formation and accelerate atherosclerosis in the early stage, whereas the proliferation of VSMCs in the late stage of plaque can prevent rupture of the fibrous cap and stabilize plaque.[46] Activation of STAT3 intensifies the proliferation of VSMCs,

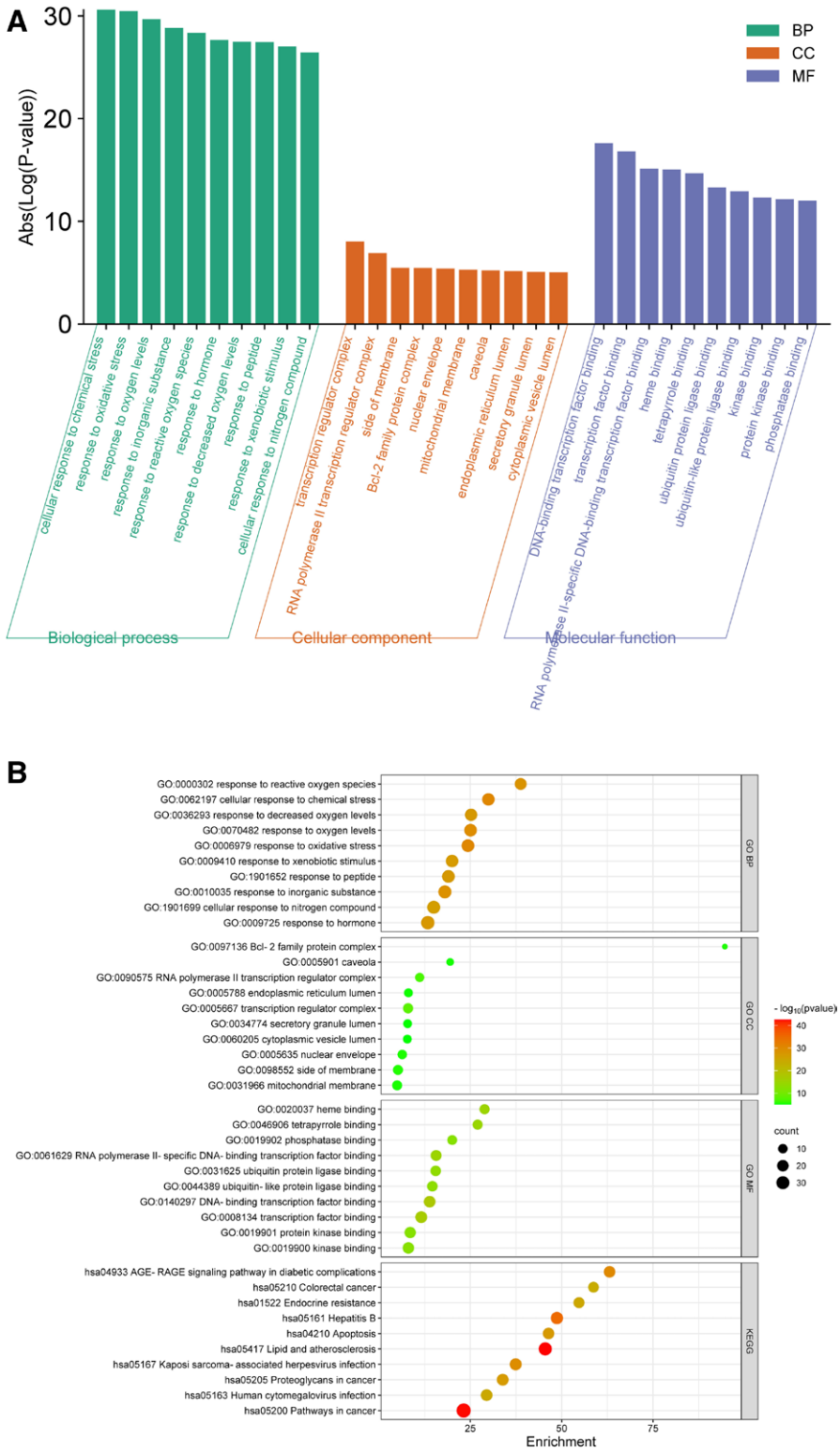

Figure 5. Enrichment analysis of YTG anti-CAD. (A) Bar charts of GO analysis, (B) Bubble charts of GO analysis and KEGG pathway analysis. There were 4 items analyzed: GO biological process, GO cellular component, GO molecular function, and KEGG pathway, listed from top to bottom. Each analysis included only the ten gene functions or participating pathways with the highest probabilities. CAD = coronary artery disease, GO = gene ontology, KEGG = Kyoto Encyclopedia of Genes and Genomes, YTG = Yixin Tongmai Granules.

while inhibiting of STAT3 significantly reduces cell proliferation.[47] Therefore, STAT3 plays a crucial role in the progression of atherosclerosis. Research by Kim et al showed that, STAT3 is hyperphosphorylated in human oral squamous cell carcinoma, and cryptotanshinone can strongly inhibit the activity of STAT3 by dephosphorylation of STAT3, which presents good antitumor activity by decreasing cell viability and inducing apoptosis.[48] The researches of Wang et al[49] and Li et al[50] on the treatment of different tumors with cryptotanshinone reached the same conclusion. Since abnormal activation of STAT3 has been shown to

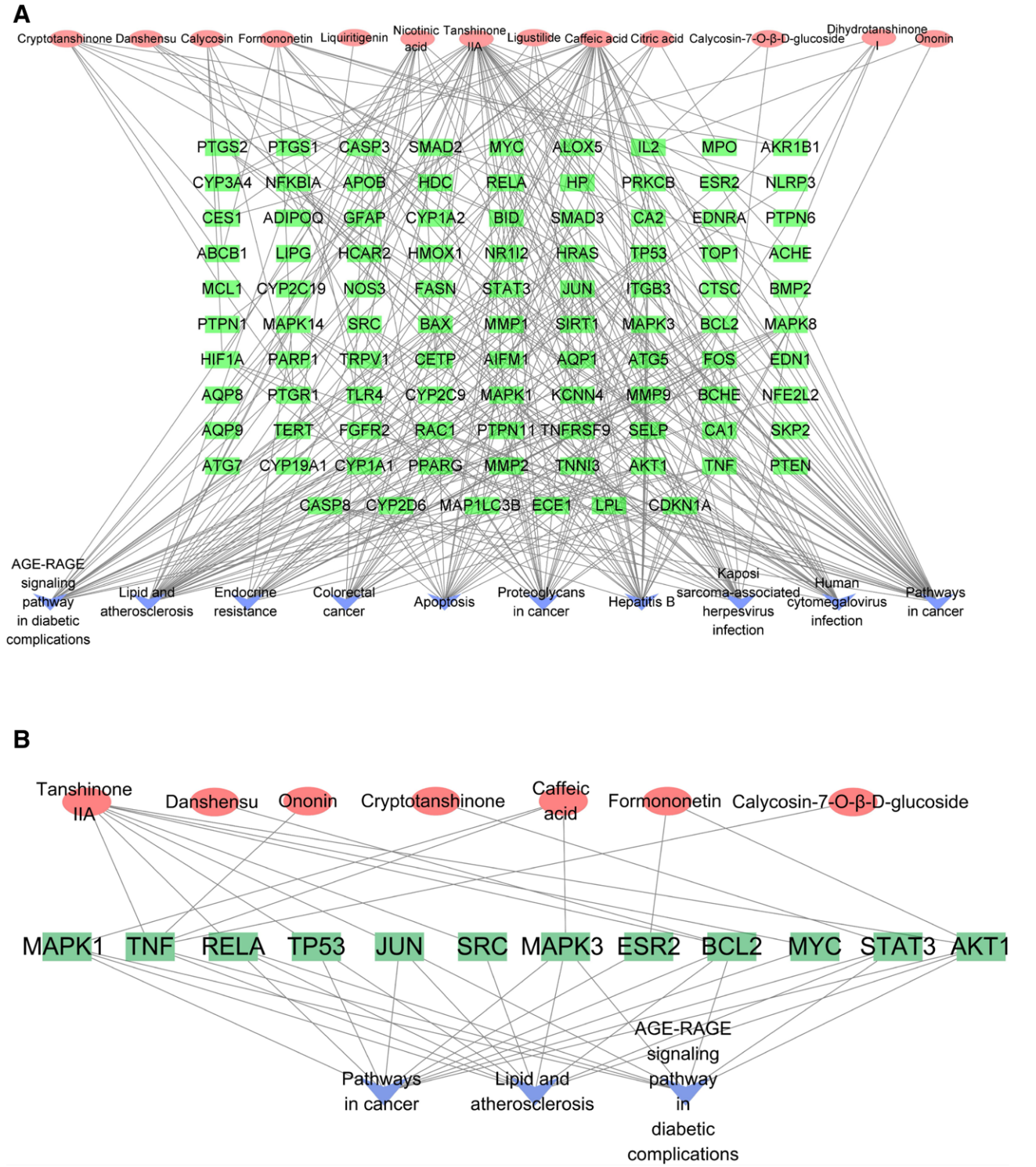

Figure 6. Association analysis between ingredients, targets and pathways for YTG. (A) Network diagram of "Effective Ingredients vs. Effective Targets vs. High *P*-value Pathways" for YTG, (B) Network diagram of "Core Ingredients vs. Core Targets vs. Principal Pathways" for YTG. YTG = Yixin Tongmai Granules.

contribute to the occurrence and development of atherosclerosis, and cryptotanshinone in YTG is a direct and very effective inhibitor of STAT3, which is supported by the literature, this study suggests that cryptotanshinone inhibiting STAT3 may be an important way for YTG to resist atherosclerosis.

AKT1, a member of the AKT kinase family (AKT1, AKT2 and AKT3), can be activated by diverse biochemical factors that regulate many biological processes, including metabolism, proliferation, cell survival, growth, and angiogenesis, which are mediated through the phosphorylation of downstream substrates.[51] Fernández-Hernando et al found that deletion of AKT1 accelerates atherosclerosis in APOE$^{-/-}$mice owing to the up regulation of pro-inflammatory genes and the apoptosis of endothelial cells and macrophages.[52] Fernández-Hernando et al further showed that the migration and survival of VSMCs decreases, the plaque is prone to rupture, and severe cardiovascular diseases such as myocardial infarction may occur in the presence of atherosclerosis and absence of AKT1.[53] Activation

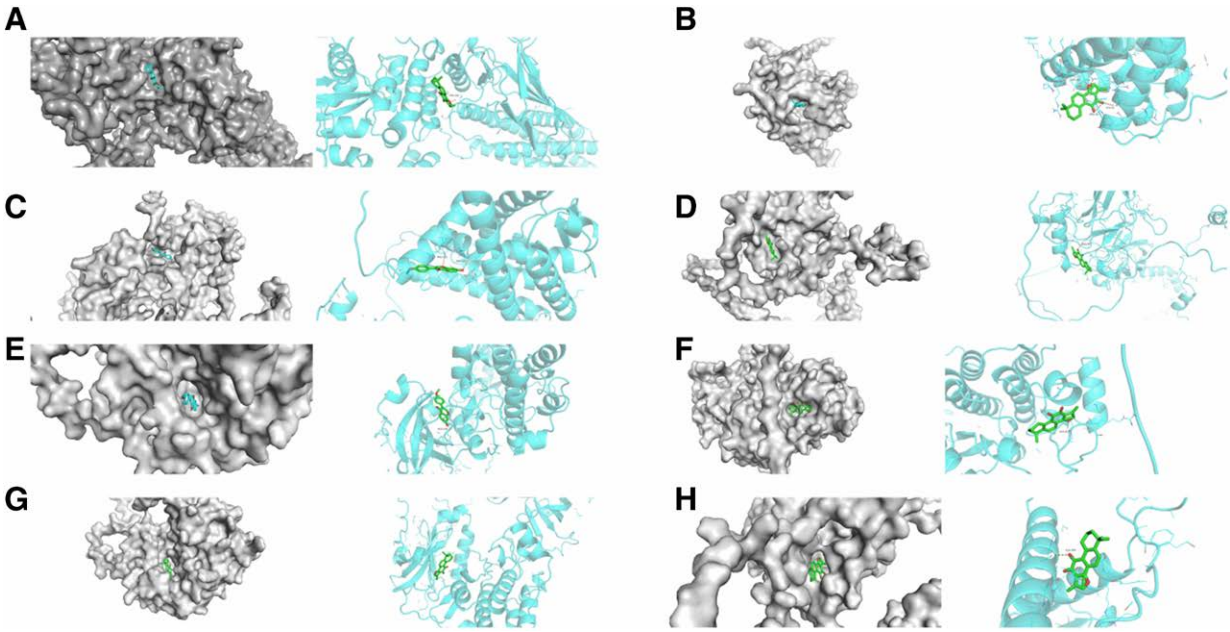

Figure 7. 3D visual simulation of the molecule docking with top scores. (A) Cryptotanshinone and STAT3, (B) Tanshinone IIA and BCL2, (C) Formononetin and ESR2, (D) Tanshinone IIA and RELA, (E) Formononetin and AKT1, (F) Tanshinone IIA and SRC, (G) Tanshinone IIA and AKT1, (H) Tanshinone IIA and TP53. This figure illustrates the 3D docking conformations between the 8 molecular ingredients and the 8 target proteins, using 2 representations: the surface model and the ribbon model. Among the surface models, the gray area in each image represents the 3D surface profile of the target protein, while the blue or green sections illustrate the stick structure of its ingredients. Among the ribbon models, the blue sections in each image represent the 3D surface profile of the target protein, the green sections depict the stick structure of the ingredient, and the yellow sections illustrate the hydrogen bonds formed between the ingredient and the protein. BCL2 = B-cell lymphoma-2, ESR2 = estrogen receptor 2, RELA = transcription factor p65, STAT3 = signal transducer and activator of transcription 3, TP53 = tumor protein 53.

Table 4

Multi-source data integration of the core ingredients and the core targets.

Ligand	Content in YK(%)	Receptor	The data from the HIT database			Docking affinity (kcal/mol)
			Target level	Target type	PMID of PubMed	
Calycosin-7-O-β-D-glucoside	0.65	TNF	N/A	N/A	N/A	−6.7
Tanshinone IIA		SRC	C	Down regulate	15081864	−10.1
		AKT1	A	Direct inhibit	23437233	−7.9
		JUN	A	Direct inhibit	20109438; 17979138; 18619357	−6.3
		TP53	C	Up regulate	18622903	−7.4
		MYC	C	Down regulate	16104505	−6.5
		RELA	A	Direct inhibit	16797002; 17979138	−6.9
		TNF	A	Direct inhibit	21722522	−6.4
		BCL2	C	Down regulate	16104505; 16104505	−7.1
Caffeic acid	3.539	MAPK1	B	Binder	25104643	−5.1
		MAPK3	B	Binder	25104643	−6.0
		TNF	C	Others	12182233	−5.7
Cryptotanshinone	13.353	STAT3	A	Direct–inhibitor	29207645; 31452742	−8.2
Formononetin	0.984	AKT1	B	Binder	26575424	−8.1
		ESR2	A	Direct inhibit	11824555	−8.1
Ononin	1.623	TNF	N/A	N/A	N/A	−6.8
Danshensu	3.269	BCL2	C	Up regulate	23139821	−4.1

JUN = transcription factor Jun, MAPK1 = MAP kinase-activated protein kinase 1, MAPK3 = MAP kinase-activated protein kinase 3, MYC = myelocytomatosis, PPI = protein–protein interaction, RELA = transcription factor p65, SRC = c-Src, STAT3 = signal transducer and activator of transcription 3, TNF = tumor necrosis factor, TP53 = tumor protein 53.

of AKT1 requires phosphorylation of its site Thr^{308} at least. If Ser^{473} is also phosphorylated, it will further enhance the catalytic activity.[54] Babaev et al confirmed that suppression phosphorylation of Ser^{473} can decrease cell viability and early atherosclerosis.[55] Luo et al showed that Tanshinone IIA at 10 mg/mL significantly inhibited hypoxia-induced phosphorylation of AKT, but had no significant effect on total AKT.[56] Therefore, this study suggests that Tanshinone IIA suppresses atherosclerosis by inhibition the phosphorylation of AKT1. In addition, Wu et al showed that formononetin could clearly reduce FGF2-triggered activation of FGFR2 and subsequent phosphorylation of AKT (Thr^{308}) in a concentration-dependent manner, while the overall levels of AKT did not markedly change.[57] Therefore, this study also suggests that formononetin in YTG can resist atherosclerosis via AKT signaling.

MAPK1, also known as ERK2, is activated by dually phosphorylated Thr^{185} and Tyr^{187}, which are involved in regulating life activities such as cell growth, adhesion, meiosis, mitosis,

survival, and differentiation. Zhu et al found that MAPK1 is up regulated in CAD, and positively affects CAD progresses.[58] Yang et al showed that caffeic acid can inhibit MAPK1 kinase activity by directly binding to MAPK1 in an ATP competitive manner.[59] So this study suggests that caffeic acid has potential application prospects in the treatment of CAD.

c-Src (SRC) is a member of the Src family of tyrosine kinases and is widely expressed in the human body. The main components of atherosclerotic plaques are lipids, which contain high levels of cholesterol and other lipids. Plaque formation leads to vascular stenosis or even occlusion. The expression of TLR4 and SRC in atherosclerotic tissue is up regulated, and oxidized low-density lipoprotein can induce TLR4 activating SRC and trigger macrophage lipid accumulation.[60] Kim et al showed that the adding of tanshinone IIA to osteoclast precursor cultures resulted in significant downregulation of SRC.[61] Therefore, this study suggests that tanshinone IIA may alleviate lipid accumulation in atherosclerosis by decreasing SRC.

The apoptotic regulator BCL2 acts as an inhibitor of apoptosis and autophagy. Thorp et al found that BCL2 deficiency in macrophages may lead to advanced lesional macrophage apoptosis.[62] Ku et al confirmed that BCL2 is the main anti apoptotic factor that determines macrophage survival.[63] Hu et al showed that the expression of BCL2 in tumor cells remarkably decreased in vitro after processing with tanshinone IIA for 2 days.[64] Huang et al confirmed that tanshinone IIA can suppress the expression of BCL2 in tumor cells in vitro.[65] In addition, Li et al found that danshensu can up regulate the expression of BCL2 and reduce myocardial injury induced by isoproterenol in vivo.[66] Therefore, this study suggests that tanshinone IIA and danshensu are mutually antagonistic in the treatment of arteriosclerosis from the perspective of macrophage apoptosis.

NF-κB is a heterodimer or homodimer protein complex composed of 5 family members (NFKB1, NFKB2, RELA, RELB, and c-REL) that manipulates DNA transcription, cytokine production, and cell survival. NF-κB plays a key role in the regulation of immune responses and inflammation and is highly associated with the pathogenesis and progression of various cardiovascular diseases and arteriosclerosis.[67] Tanshinone IIA can inhibit the increase in NF-κB and DNA complex, and NF-κB binding activity in a dose-dependent manner to generate anti-inflammatory effects.[68] Additionally, Jin et al also showed that tanshinone IIA can inhibited NF-κB and AP-1 DNA-binding.[69]

TP53 is a tumor suppressor gene. Bensaad et al found that TP53 could induce the expression of TIGAR to inhibit glycolysis and decrease the level of intracellular active oxygen.[70] Zhao et al further found that TIGAR could mitigate the development of atherosclerosis by promoting cholesterol efflux from macrophages.[71] Su et al showed that tanshinone IIA increases the expression of TP53.[72] Therefore, this study suggests that tanshinone IIA may up regulate the expression of TP53 thus indirectly resisting atherosclerosis to a certain extent.

TNF is a cytokine that is mainly expressed by macrophages when injured and stimulated, and has biological functions in inflammatory response regulation, immunoregulation, and cytotoxicity by inducing apoptosis.[73] TNF increases LDL transcytosis across endothelial cells and thus facilitates LDL retention in the vascular wall; hence, it plays an important role in atherosclerosis.[74] The level of TNF significantly increases with acute ischemia, and plasma concentrations of TNF are persistently elevated in patients with myocardial infarction.[75] Additionally, TNF is a key aging-related pro-inflammatory cytokine that leads to platelet hyperreactivity and increases the risk of thrombus.[76] Therefore, TNF may be a promising treatment target for CAD and its complications. Some core ingredients in YTG target TNF. Jia et al found that tanshinone IIA inhibits the upregulation of LPS-induced TNF.[77] Giovannini et al showed that caffeic acid could inhibit the release of LPS-induced TNF.[78] Xu et al also showed that ononin could inhibit IL-1β-induced upregulation of TNF in a dose-dependent manner.[79] Moreover, Li et al showed that Calycosin-7-O-β-D-glucoside could not inhibit LPS-induced upregulation of TNF.[80] Therefore, tanshinone IIA, caffeic acid, and ononin have an inhibitory effect on TNF.

E2 is an endogenous steroid hormone and is the main female sex hormone. ERα (ESR1) and ERβ(ESR2) are important members of the E2 receptor family. There is no consensus regarding the treatment of CAD in postmenopausal women with E2 targeting ESR2. Geraldes et al found that E2 might activate ESR2 to decrease the migration and proliferation of smooth muscle cells.[81] However, Mcrobb et al showed that E2 could suppress the expression of ESR2 and drive calcification by metaplasia from VSMCs to osteoblast-like cells in advanced atherosclerotic lesions.[82] Morito showed that formononetin binds well to ESR2 and acts as an antagonist of the induction of transcription by E2.[83]

c-Jun (JUN) is a kind of proto-oncogene protein that often binds to FOS or FOSB to form an AP-1 transcription factor complex. Zhong et al found that the knockout of JUN produces unexpected positive effects of inducing differentiation from human pluripotent stem cells to cardiomyocytes in vitro.[84] Therefore, anti-JUN therapy may have a promising application prospect in myocardial regeneration. Jin et al found that tanshinone IIA could suppress TNF-induced c-jun phosphorylation.[69] Moreover, Zhou et al showed that tanshinone IIA could alleviate Angiotensin II-induced cardiomyocyte hypertrophy by inhibiting the mRNA expression of FOS and JUN.[85]

MAPK3, also known as ERK1, is activated by dually phosphorylated Thr^{202} and Tyr^{204}, and its function is similar to that of MAPK1. Chen et al based on gene GEO showed that MAPK3 was relatively down regulated in the atherosclerotic group compared to the normal group.[86] Yang et al showed that caffeic acid can dose-dependently inhibit MAPK3 kinase activities.[59]

c-Myc (MYC) is a proto-oncogene that functions as a transcription factor and regulates the expression of multiple genes. Wang et al based on GEO showed that MYC and MYC-mediated downstream targets were down regulated in heart failure tissues,[87] it can be inferred that MYC plays a key role in heart failure. Hu et al showed that the expression of MYC remarkably decreased in vitro after being processed with tanshinone IIA 2 days.[64]

4.2. Literatures related to effective ingredients

Tanshinone IIA is a fat-soluble diterpene quinone found in danshen. It has a variety of biological activities, including antioxidant, anti-inflammatory, anticoagulant, antithrombotic, neuroprotective, immunoregulatory, and antitumor activities, as well as extraordinary cardioprotective effects by enhancing angiogenesis.[88] Caffeic acid is a phenolic acid component that is shared by renshen, beishashen, danshen and chuanxiong. It has a variety of biological activities, including antioxidant, anti-inflammatory, antibacterial, cytostatic and vasorelaxant.[89] Nicotinic acid is a heterocyclic ingredient in huangqi and is 1 of the 13 essential vitamins in the human body. It can improve blood lipid abnormalities by increasing plasma high-density lipoprotein cholesterol concentration.[90] Formononetin is a flavonoid shared by zhigancao, huangqi, and danshen. It has biological activities, such as antioxidation, antihypertension, antitumor, anti-infection, and neuroprotection.[91] Liquiritin is a flavonoid extracted from zhigancao. It has anti-inflammatory and cardioprotective properties.[92] Danshensu, with an alias of salvianic acid A, is a phenolic acid ingredient in danshen. It mainly shows therapeutic effects in some cardiovascular diseases such as myocardial I/R, atherosclerosis, and hypertension.[93] Cryptotanshinone is a fat-soluble diterpene quinone extracted from danshen. Cryptotanshinone has 2 optical isomers (PubChem CID:160254 and PubChem CID:25181389).

According to data from the HIT database, cryptotanshinone in danshen is the first isomer. It has a variety of biological activities, including anticancer, anti-inflammatory, immune regulation, neuroprotective, and antifibrosis.[94] Liu et al found that cryptotanshinone had anti-atherosclerotic activity.[95] Ahmad[96] found that cryptotanshinone could significantly suppress TNF-induced endothelial cell activation and prevent cytokine-induced early atherogenesis via anti-inflammatory activity. Calycosin is a flavonoid present in huangqi. It has been reported to have anticancer, antioxidative, immunomodulatory, and estrogenic-like properties.[97] Citric acid is a type of organic acid in renshen, which generally improves appetite. It has protective effects against myocardial I/R injury, which are based on anti-inflammatory, antiplatelet aggregation, and direct cardiomyocyte protective effects.[98] Dihydrotanshinone I is a phenanthraquinones present in danshen. It could inhibit angiogenesis by suppressing endothelial cell proliferation, migration, invasion and tube formation.[99] Ligustilide is a terpenoid found in chuanxiong. It has neuroprotective effects against neurodegenerative diseases.[100] In addition, it has the biological activity of anticancer based on inhibiting tumor angiogenesis.[101] Ononin is an isoflavone shared by zhigancao and huangqi. It can inhibit angiogenesis, thereby restraining tumor growth.[102] It has anti-inflammatory activity in lipopolysaccharide-induced inflammatory responses.[103] It has antifungal activity against Candida albicans and may be an alternative drug for this disease.[104] Calycosin-7-O-β-D-glucoside is an isoflavone present in huangqi. It may alleviate I/R injury.[105] It can significantly improve cell viability and reduce oxidative stress and neuronal apoptosis.[106] Liquiritigenin is a flavonoid extracted from zhigancao. It has antifibrotic properties.[107]

5. Conclusion

TCM is mostly based on traditional medical experiences, and is derived from a combination of natural drugs. However, the chemical composition of a drug is very complex, often comprising hundreds or even thousands ingredients. These ingredients can act on multiple targets and exert a variety of pharmacological effects. In addition, there are interactions between some targets and synergy and antagonism between some ingredients. Moreover, the content of ingredients in 1 TCM drug may be high or low, leading to changes in the pharmacodynamics. Therefore, the pharmacology of TCM is complex. In this study, the ingredients of YTG were identified based on more rigorous experimental UHPLC-MS/MS data. The active ingredients were screened based on the content threshold (not <0.5%) and the ADME criteria of the SwissADME platform. Then, the HIT database and SwissTargetPrediction platform were used to search for high-confidence targets from 2 aspects, namely, literature support and chemical structure similarity. After the drug and disease targets of CAD were imported into Venny 2.1, the effective targets of YTG were obtained. PPI analysis of the above targets was carried out using STRING, and the core targets of YTG were derived, which were TP53, STAT3, JUN, MAPK3, MAPK1, AKT1, SRC, MYC, BCL2, RELA, TNF, and ESR2. Next, 96 effective targets were imported into Metascape. Through enrichment analysis of the effective targets, ten biological processes, ten cell components, ten molecular functions and ten signal pathways with high significance were identified. After analysis, the top pathways associated with CAD are "Lipid and atherosclerosis," "Pathways in cancer," and "AGE-RAGE signaling pathway in diabetic complications." Using Cytoscape, this study built a biological network diagram of YTG in the treatment of CAD, between the effective ingredients, effective targets, and high *P*-value pathways (core ingredients, core targets, and principal pathways). AutoDock and PyMOL were used to carry out molecular docking and visualization of the core ingredients and core targets to evaluate the affinity between them. Finally, by analyzing and summarizing related literature, mainly recommended by the HIT database, this study explored the molecular mechanism of YTG in treating CAD from ingredients, targets and CAD, and inferred the main pharmacological ingredients of YTG, namely tanshinone IIA, cryptotanshinone, caffeic acid, denshensu, ononin, and formononetin. The pharmacology of the effective ingredients in the literature has also been arranged as a supplement to the former. The data and analysis in this study, particularly anti-arteriosclerosis pharmacologies of YTG, are helpful for scholars to comprehensively understand the complex pharmacological mechanism of YTG against CAD and its complications.

Author contributions

Data curation: Yuye Zhu.
Formal analysis: Hongbin Li.
Funding acquisition: Hongbin Li.
Methodology: Hongbin Li.
Project administration: Yuye Zhu.
Resources: Hongbin Li.
Writing – original draft: Hongbin Li.
Writing – review & editing: Yuye Zhu.

References

[1] GBD 2016 Disease and Injury Incidence and Prevalence Collaborators. Global, regional, and national incidence, prevalence, and years lived with disability for 328 diseases and injuries for 195 countries, 1990-2016: a systematic analysis for the Global Burden of Disease Study 2016. Lancet. 2017;390:1211–59.

[2] Arnett DK, Blumenthal RS, Albert MA, et al. 2019 ACC/AHA Guideline on the primary prevention of cardiovascular disease: executive summary: a report of the American College of Cardiology/American Heart Association task force on clinical practice guidelines. J Am Coll Cardiol. 2019;74:1376–414.

[3] Higgins M. Epidemiology and prevention of coronary heart disease in families. Am J Med. 2000;108:387–95.

[4] Mahmood H, Siddique I, McKechnie A. Antiplatelet drugs: a review of pharmacology and the perioperative management of patients in oral and maxillofacial surgery. Ann R Coll Surg Engl. 2019;102:9–13.

[5] Ruscica M, Ferri N, Santos RD, Sirtori CR, Corsini A. Lipid lowering drugs: present status and future developments. Curr Atheroscler Rep. 2021;23:17.

[6] Brown T, Gonzalez J, Monteleone C. Angiotensin-converting enzyme inhibitor-induced angioedema: a review of the literature. J Clin Hypertens (Greenwich). 2017;19:1377–82.

[7] Elliott WJ, Ram CVS. Calcium channel blockers. J Clin Hypertens (Greenwich). 2011;13:687–9.

[8] Fumagalli C, Maurizi N, Marchionni N, Fornasari D. β-blockers: their new life from hypertension to cancer and migraine. Pharmacol Res. 2020;151:104587.

[9] Tarkin JM, Kaski JC. Vasodilator therapy: nitrates and nicorandil. Cardiovasc Drugs Ther. 2016;30:367–78.

[10] Toma MM, Bungau SG, Tit DM, et al. Use of anticoagulant drugs in patients with atrial fibrillation. Does adherence to therapy have a prognostic impact? Biomed Pharmacother. 2022;150:113002.

[11] Marti C, John G, Konstantinides S, et al. Systemic thrombolytic therapy for acute pulmonary embolism: a systematic review and meta-analysis. Eur Heart J. 2015;36:605–14.

[12] Tian Y, Pei S, Xiao C, et al. Yixin Tongmai granules. CN103007201A. 2013. https://kns.cnki.net/kcms2/article/abstract?v=Hk3u3f8a_QvG5N8higen_Gwy7HNy5FqQelcT0CQ9l_2BUCbObul1GeR_ljKJZyqxy41qGixLYuPcH4yGu3Y9VDR88B_RV9qsqXP8DlSrrcyS0BkmixPldu2sL8zcER1W595nV_OvHeT_qtIQV37eRdvT7TuUCwTLhzethdyyyCHYWQMsG_NnuK2snWCryKAk&uniplatform=NZKPT&language=CHS.

[13] Su R, He Y. Effect of Yixin Tongmai Grains on Qi and blood stasis after intervention therapy for coronary heart disease. Chin J Exp Tradit Med Formulae. 2017;23:201–6.

[14] Hopkins AL. Network pharmacology. Nat Biotechnol. 2007;25:1110–1.

[15] Pinzi L, Rastelli G. Molecular docking: shifting paradigms in drug discovery. Int J Mol Sci. 2019;20:4331.

[16] Gupta R, Srivastava D, Sahu M, Tiwari S, Ambasta RK, Kumar P. Artificial intelligence to deep learning: machine intelligence approach for drug discovery. Mol Divers. 2021;25:1315–60.
[17] Holmes SG, Desai UR. Assessing genetic algorithm-based docking protocols for prediction of heparin oligosaccharide binding geometries onto proteins. Biomolecules. 2023;13:1633.
[18] Yue SY. Distance-constrained molecular docking by simulated annealing. Protein Eng. 1990;4:177–84.
[19] Barros RC, Winck AT, Machado KS, et al. Automatic design of decision-tree induction algorithms tailored to flexible-receptor docking data. BMC Bioinf. 2012;13:310.
[20] Daina A, Michielin O, Zoete V. SwissADME: a free web tool to evaluate pharmacokinetics, drug-likeness and medicinal chemistry friendliness of small molecules. Sci Rep. 2017;7:42717.
[21] Yan D, Zheng G, Wang C, et al. HIT 2.0: an enhanced platform for herbal ingredients' targets. Nucleic Acids Res. 2022;50:D1238–43.
[22] Gfeller D, Grosdidier A, Wirth M, Daina A, Michielin O, Zoete V. SwissTargetPrediction: a web server for target prediction of bioactive small molecules. Nucleic Acids Res. 2014;42:W32–8.
[23] Rebhan M, Chalifa-Caspi V, Prilusky J, Lancet D. GeneCards: a novel functional genomics compendium with automated data mining and query reformulation support. Bioinformatics. 1998;14:656–64.
[24] Shannon P, Markiel A, Ozier O, et al. Cytoscape: a software environment for integrated models of biomolecular interaction networks. Genome Res. 2013;13:2498–504.
[25] SzklarczYTG D, Franceschini A, Wyder S, et al. STRING v10: protein-protein interaction networks, integrated over the tree of life. Nucleic Acids Res. 2015;43:D447–52.
[26] Tang Y, Li M, Wang J, Pan Y, Wu F-X. CytoNCA: a cytoscape plugin for centrality analysis and evaluation of protein interaction networks. Biosystems. 2015;127:67–72.
[27] Zhou Y, Zhou B, Pache L, et al. Metascape provides a biologist-oriented resource for the analysis of systems-level datasets. Nat Commun. 2019;10:1523.
[28] Buntrock RE. ChemOffice ultra 7.0. J Chem Inf Comput Sci. 2002;42:1505–6.
[29] UniProt Consortium T. UniProt: the universal protein knowledgebase. Nucleic Acids Res. 2018;46:2699.
[30] Morris GM, Huey R, Lindstrom W, et al. AutoDock4 and AutoDockTools4: automated docking with selective receptor flexibility. J Comput Chem. 2009;30:2785–91.
[31] Trott O, Olson AJ. AutoDock Vina: improving the speed and accuracy of docking with a new scoring function, efficient optimization, and multithreading. J Comput Chem. 2010;31:455–61.
[32] Seeliger D, de Groot BL. Ligand docking and binding site analysis with PyMOL and Autodock/Vina. J Comput Aided Mol Des. 2010;24:417–22.
[33] Lusis AJ. Atherosclerosis. Nature. 2000;407:233–41.
[34] Weber C, Noels H. Atherosclerosis: current pathogenesis and therapeutic options. Nat Med. 2011;17:1410–22.
[35] Li J, Zhao J, Lei Y, et al. Coronary atherosclerotic disease and cancer: risk factors and interrelation. Front Cardiovasc Med. 2022;9:821267.
[36] Ellis RW. Infection and coronary heart disease. J Med Microbiol. 1997;46:535–9.
[37] Du Y, Zhang G, Liu Z. Human cytomegalovirus infection and coronary heart disease: a systematic review. Virol J. 2018;15:31.
[38] Wijarnpreecha K, Thongprayoon C, Panjawatanan P, Ungprasert P. Hepatitis B virus infection and risk of coronary artery disease: a meta-analysis. Ann Transl Med. 2016;4:423.
[39] Naito R, Miyauchi K. Coronary artery disease and type 2 diabetes mellitus. Int Heart J. 2017;58:475–80.
[40] Dong Y, Chen H, Gao J, Liu Y, Li J, Wang J. Molecular machinery and interplay of apoptosis and autophagy in coronary heart disease. J Mol Cell Cardiol. 2019;136:27–41.
[41] Du Y, Du L, He Z, Zhou J, Wen C, Zhang Y. Cryptotanshinone ameliorates the pathogenesis of systemic lupus erythematosus by blocking T cell proliferation. Int Immunopharmacol. 2019;74:105677.
[42] Guanizo AC, Fernando CD, Garama DJ, Gough DJ. STAT3: a multifaceted oncoprotein. Growth factors. 2018;36:1–14.
[43] Wei Z, Jiang W, Wang H, et al. The IL-6/STAT3 pathway regulates adhesion molecules and cytoskeleton of endothelial cells in thromboangiitis obliterans. Cell Signal. 2018;44:118–26.
[44] Chen Q, Lv J, Yang W, et al. Targeted inhibition of STAT3 as a potential treatment strategy for atherosclerosis. Theranostics. 2019;9:6424–42.
[45] Vasamsetti SB, Karnewar S, Kanugula AK, Thatipalli AR, Kumar JM, Kotamraju S. Metformin inhibits monocyte-to-macrophage differentiation via AMPK-mediated inhibition of STAT3 activation: potential role in atherosclerosis. Diabetes. 2015;64:2028–41.
[46] Bennett MR, Sinha S, Owens GK. Vascular smooth muscle cells in atherosclerosis. Circ Res. 2016;118:692–702.
[47] Liao XH, Wang N, Zhao DW, et al. STAT3 protein regulates vascular smooth muscle cell phenotypic switch by interaction with myocardin. J Biol Chem. 2015;290:19641–52.
[48] Kim LH, Khadka S, Shin JA, et al. Nitidine chloride acts as an apoptosis inducer in human oral cancer cells and a nude mouse xenograft model via inhibition of STAT3. Oncotarget. 2017;8:91306–15.
[49] Wang J, Zhang G, Dai C, et al. Cryptotanshinone potentiates the antitumor effects of doxorubicin on gastric cancer cells via inhibition of STAT3 activity. J Int Med Res. 2017;45:220–30.
[50] Li W, Saud SM, Young MR, Colburn NH, Hua B. Cryptotanshinone, a Stat3 inhibitor, suppresses colorectal cancer proliferation and growth in vitro. Mol Cell Biochem. 2015;406:63–73.
[51] Nicholson KM, Anderson NG. The protein kinase B/Akt signalling pathway in human malignancy. Cell Signal. 2002;14:381–95.
[52] Fernández-Hernando C, Ackah E, Yu J, et al. Loss of Akt1 leads to severe atherosclerosis and occlusive coronary artery disease. Cell Metab. 2007;6:446–57.
[53] Fernández-Hernando C, József L, Jenkins D, Di Lorenzo A, Sessa WC. Absence of Akt1 reduces vascular smooth muscle cell migration and survival and induces features of plaque vulnerability and cardiac dysfunction during atherosclerosis. Arterioscler Thromb Vasc Biol. 2009;29:2033–40.
[54] Balasuriya N, McKenna M, Liu X, Li SSC, O'Donoghue P. Phosphorylation-dependent inhibition of Akt1. Genes. 2018;9:450.
[55] Babaev VR, Ding L, Zhang Y, et al. Macrophage IKKα deficiency suppresses Akt phosphorylation, reduces cell survival, and decreases early atherosclerosis. Arterioscler Thromb Vasc Biol. 2016;36:598–607.
[56] Luo Y, Xu DQ, Dong HY, et al. Tanshinone IIA inhibits hypoxia-induced pulmonary artery smooth muscle cell proliferation via Akt/Skp2/p27-associated pathway. PLoS One. 2013;8:e56774.
[57] Wu XY, Xu H, Wu ZF, et al. Formononetin, a novel FGFR2 inhibitor, potently inhibits angiogenesis and tumor growth in preclinical models. Oncotarget. 2015;6:44563–78.
[58] Zhu Y, Yang T, Duan J, Mu N, Zhang T. MALAT1/miR-15b-5p/MAPK1 mediates endothelial progenitor cells autophagy and affects coronary atherosclerotic heart disease via mTOR signaling pathway. Aging (Milano). 2019;11:1089–109.
[59] Yang G, Fu Y, Malakhova M, et al. Caffeic acid directly targets ERK1/2 to attenuate solar UV-induced skin carcinogenesis. Cancer Prev Res (Phila). 2014;7:1056–66.
[60] Yang K, Wang X, Liu Z, et al. Oxidized low-density lipoprotein promotes macrophage lipid accumulation via the toll-like receptor 4-Src pathway. Circ J. 2015;79:2509–16.
[61] Kim HH, Kim JH, Kwak HB, et al. Inhibition of osteoclast differentiation and bone resorption by tanshinone IIA isolated from Salvia miltiorrhiza Bunge. Biochem Pharmacol. 2004;67:1647–56.
[62] Thorp E, Li Y, Bao L, et al. Brief report: increased apoptosis in advanced atherosclerotic lesions of Apoe-/- mice lacking macrophage Bcl-2. Arterioscler Thromb Vasc Biol. 2009;29:169–72.
[63] Ku B, Liang C, Jung JU, Oh B-H. Evidence that inhibition of BAX activation by BCL-2 involves its tight and preferential interaction with the BH3 domain of BAX. Cell Res. 2011;21:627–41.
[64] Hu H, Zhang Y, Huang F, et al. Inhibition of proliferation and induction of apoptosis by Tanshinone IIA in NCI-H460 cell. J Chin Med Mater. 2005;28:301–4.
[65] Huang J, Lin H, Hong Y. In vitro anti-tumor activity of the tanshinone IIA against SKOV3 cells. Nat Prod Res. 2016;30:1844–6.
[66] Li H, Xie YH, Yang Q, et al. Cardioprotective effect of paeonol and danshensu combination on isoproterenol-induced myocardial injury in rats. PLoS One. 2012;7:e48872.
[67] Matsumori A. Nuclear factor-κB is a prime candidate for the diagnosis and control of inflammatory cardiovascular disease. Eur Cardiol. 2023;18:e40.
[68] Jang SI, Kim HJ, Kim YJ, Jeong S-I, You Y-O. Tanshinone IIA inhibits LPS-induced NF-kappaB activation in RAW 264.7 cells: possible involvement of the NIK-IKK, ERK1/2, p38 and JNK pathways. Eur J Pharmacol. 2006;542:1–7.
[69] Jin UH, Suh SJ, Chang HW, et al. Tanshinone IIA from Salvia miltiorrhiza BUNGE inhibits human aortic smooth muscle cell migration and MMP-9 activity through AKT signaling pathway. J Cell Biochem. 2008;104:15–26.
[70] Bensaad K, Tsuruta A, Selak MA, et al. TIGAR, a p53-inducible regulator of glycolysis and apoptosis. Cell. 2006;126:107–20.

[71] Zhao ZW, Zhang M, Zou J, et al. TIGAR mitigates atherosclerosis by promoting cholesterol efflux from macrophages. Atherosclerosis. 2021;327:76–86.
[72] Su CC, Chen GW, Kang JC, Chan M-H. Growth inhibition and apoptosis induction by tanshinone IIA in human colon adenocarcinoma cells. Planta Med. 2008;74:1357–62.
[73] Diaz Arguello OA, Haisma HJ. Apoptosis-inducing TNF superfamily ligands for cancer therapy. Cancers. 2021;13:1543.
[74] Zhang Y, Yang X, Bian F, et al. TNF-α promotes early atherosclerosis by increasing transcytosis of LDL across endothelial cells: crosstalk between NF-κB and PPAR-γ. J Mol Cell Cardiol. 2014;72:85–94.
[75] Ridker PM, Rifai N, Pfeffer M, Sacks F, Lepage S, Braunwald E. Braunwald E. Elevation of tumor necrosis factor-alpha and increased risk of recurrent coronary events after myocardial infarction. Circulation. 2000;101:2149–53.
[76] Davizon-Castillo P, McMahon B, Aguila S, et al. TNF-α-driven inflammation and mitochondrial dysfunction define the platelet hyperreactivity of aging. Blood. 2019;134:727–40.
[77] Jia LQ, Feng JY, Yang GL, et al. Effect of tanshinone II A on TLR4 and TNF-α of endothelial cells induced by LPS. Chin J Cell Mol Immunol. 2011;27:733–5.
[78] Giovannini L, Migliori M, Filippi C, et al. Inhibitory activity of the white wine compounds, tyrosol and caffeic acid, on lipopolysaccharide-induced tumor necrosis factor-alpha release in human peripheral blood mononuclear cells. Int J Tissue React. 2002;24:53–6.
[79] Xu F, Zhao LJ, Liao T, et al. Ononin ameliorates inflammation and cartilage degradation in rat chondrocytes with IL-1β-induced osteoarthritis by downregulating the MAPK and NF-κB pathways. BMC Complement Med Ther. 2022;22:25.
[80] Li W, Sun YN, Yan XT, et al. Flavonoids from Astragalus membranaceus and their inhibitory effects on LPS-stimulated pro-inflammatory cytokine production in bone marrow-derived dendritic cells. Arch Pharm Res. 2014;37:186–92.
[81] Geraldes P, Sirois MG, Tanguay JF. Specific contribution of estrogen receptors on mitogen-activated protein kinase pathways and vascular cell activation. Circ Res. 2003;93:399–405.
[82] McRobb LS, McGrath KCY, Tsatralis T, et al. Estrogen receptor control of atherosclerotic calcification and smooth muscle cell osteogenic differentiation. Arterioscler Thromb Vasc Biol. 2017;37:1127–37.
[83] Morito K, Aomori T, Hirose T, et al. Interaction of phytoestrogens with estrogen receptors alpha and beta (II). Biol Pharm Bull. 2002;25:48–52.
[84] Zhong H, Zhang R, Li G, et al. c-JUN is a barrier in hESC to cardiomyocyte transition. Life Sci Alliance. 2023;6:e202302121.
[85] Zhou DX, Liang QS, He XX, et al. Changes of c-fos, c-jun mRNA expressions in cardiomyocyte hypertrophy induced by angiotensin II and effects of tanshinone II A. China J Chin Mater Med. 2008;33:936–9.
[86] Chen Y, Zeng A, He S, et al. Autophagy-related genes in atherosclerosis. J Healthc Eng. 2021;2021:6402206.
[87] Wang H, Wang X, Xu L, Cao H. Identification of transcription factors MYC and C/EBPβ mediated regulatory networks in heart failure based on gene expression omnibus datasets. BMC Cardiovasc Disord. 2020;20:250.
[88] Guo R, Li L, Su J, et al. Pharmacological activity and mechanism of tanshinone IIA in related diseases. Drug Des Devel Ther. 2020;14:4735–48.
[89] Silva H, Lopes NMF. Cardiovascular effects of caffeic acid and its derivatives: a comprehensive review. Front Physiol. 2020;11:595516.
[90] Bodor ET, Offermanns S. Nicotinic acid: an old drug with a promising future. Br J Pharmacol. 2008;153:S68–75.
[91] Ma X, Wang J. Formononetin: a pathway to protect neurons. Front Integr Neurosci. 2022;16:908378.
[92] Zhang Y, Zhang L, Zhang Y, Xu J-J, Sun L-L, Li S-Z. The protective role of liquiritin in high fructose-induced myocardial fibrosis via inhibiting NF-κB and MAPK signaling pathway. Biomed Pharmacother. 2016;84:1337–49.
[93] Zhang J, Zhang Q, Liu G, Zhang N. Therapeutic potentials and mechanisms of the Chinese traditional medicine Danshensu. Eur J Pharmacol. 2019;864:172710.
[94] Li H, Gao C, Liu C, et al. A review of the biological activity and pharmacology of cryptotanshinone, an important active constituent in Danshen. Biomed Pharmacother. 2021;137:111332.
[95] Liu Z, Xu S, Huang X, et al. Cryptotanshinone, an orally bioactive herbal compound from Danshen, attenuates atherosclerosis in apolipoprotein E-deficient mice: role of lectin-like oxidized LDL receptor-1 (LOX-1). Br J Pharmacol. 2015;172:5661–75.
[96] Ahmad Z, Ng CT, Fong LY, et al. Cryptotanshinone inhibits TNF-α-induced early atherogenic events in vitro. J Physiol Sci. 2016;66:213–20.
[97] Gong G, Zheng Y, Yang Y, Sui Y, Wen Z. Pharmaceutical values of calycosin: one type of flavonoid isolated from astragalus. Evid Based Complement Alternat Med. 2021;2021:9952578.
[98] Tang X, Liu J, Dong W, et al. The cardioprotective effects of citric Acid and L-malic Acid on myocardial ischemia/reperfusion injury. Evid Based Complement Alternat Med. 2013;2013:820695.
[99] Bian W, Chen F, Bai L, Zhang P, Qin W. Dihydrotanshinone I inhibits angiogenesis both in vitro and in vivo. Acta Biochim Biophys Sin. 2008;40:1–6.
[100] Peng D, Wang YX, Huang TH, et al. Ligustilide improves cognitive impairment via regulating the SIRT1/IRE1α/XBP1s/CHOP pathway in vascular dementia rats. Oxid Med Cell Longev. 2022;2022:6664990.
[101] Ma J, Chen X, Chen Y, Tao N, Qin Z. Ligustilide inhibits tumor angiogenesis by downregulating VEGFA secretion from cancer-associated fibroblasts in prostate cancer via TLR4. Cancers. 2022;14:2406.
[102] Gong G, Zheng Y, Kong X, Wen Z. Anti-angiogenesis function of ononin via suppressing the MEK/Erk signaling pathway. J Nat Prod. 2021;84:1755–62.
[103] Dong L, Yin L, Zhang Y, Fu X, Lu J. Anti-inflammatory effects of ononin on lipopolysaccharide-stimulated RAW 264.7 cells. Mol Immunol. 2017;83:46–51.
[104] Silva AFD, Farias JR, Franco DCG, et al. Anti-Candida albicans activity of ononin and other secondary metabolites from platonia insignis MART. Metabolites. 2022;12:1014.
[105] Ren M, Wang X, Du G, Tian J, Liu Y. Calycosin-7-O-β-D-glucoside attenuates ischemia-reperfusion injury in vivo via activation of the PI3K/Akt pathway. Mol Med Rep. 2016;13:633–40.
[106] Yan X, Yu A, Zheng H, Wang S, He Y, Wang L. Calycosin-7-O-β-D-glucoside attenuates OGD/R-induced damage by preventing oxidative stress and neuronal apoptosis via the SIRT1/FOXO1/PGC-1α pathway in HT22 cells. Neural Plast. 2019;2019:8798069.
[107] Hua Q, Ren L. The SIRT1/Nrf2 signaling pathway mediates the anti-pulmonary fibrosis effect of liquiritigenin. Chin Med. 2024;19:12.